UC Berkeley
UC Berkeley Electronic Theses and Dissertations

Title
The Influence of Sn Orientation on the Electromigration of Idealized Lead-free Interconnects

Permalink
https://escholarship.org/uc/item/3ht3215h

Author
Linares, Xioranny

Publication Date
2015

Peer reviewed|Thesis/dissertation

eScholarship.org Powered by the California Digital Library
University of California

The Influence of Sn Orientation on the Electromigration of Idealized Lead-free Interconnects

By

Xioranny Linares

A dissertation submitted in partial satisfaction of the

requirements for the degree of

Doctor of Philosophy

in

Engineering - Materials Science and Engineering

in the

Graduate Division

of the

University of California, Berkeley

Committee in charge:

Professor J.W. Morris Jr., Chair

Professor Andrew Minor

Professor Tsu-Jae King Liu

Summer 2015

Abstract

The Influence of Sn Orientation on the Electromigration of Idealized Lead-free Interconnects

By

Xioranny Linares

Doctor of Philosophy in Materials Science and Engineering

University of California, Berkeley

Professor J.W. Morris Jr., Chair

As conventional lead solders are being replaced by Pb-free solders in electronic devices, the reliability of solder joints in integrated circuits (ICs) has become a high concern. Due to the miniaturization of ICs and consequently solder joints, the current density through the solder interconnects has increased causing electrical damage known as electromigration. Electromigration, atomic and mass migration due to high electron currents, is one of the most urgent reliability issues delaying the implementation of Pb-free solder materials in electronic devices. The research on Pb-free solders has mainly focused on the qualitative understanding of failure by electromigration. There has been little progress however, on the quantitative analysis of electromigration because of the lack of available material parameters, such as the effective charge, (z*), the driving force for electromigration. The research herein uses idealized interconnects to measure the z* of electromigration of Cu in *Sn*-3.0*Ag*-0.5*Cu* (*SAC305*) alloy under different experimental conditions. Planar SAC 305 interconnects were sandwiched between two Cu pads and subject to uniaxial current. The crystallographic orientation of Sn in these samples were characterized with electron backscatter diffraction (EBSD) and wavelength dispersive spectroscopy (WDS) before and after electromigration testing. Results indicate that samples with the c-axis aligned perpendicular to current flow, polycrystalline, and those with a diffusion barrier on the cathode side all inhibit the growth of intermetallic compounds (IMC). The effective charge values of Cu in SAC 305 under the different conditions tested were quantified for the first time and included in this dissertation. The following research is expected to help verify and improve the electromigration model and identify the desirable conditions to inhibit damage by electromigration in Pb-free solder joints.

To my family -
For loving, forgiving and supporting me even in my darkest hours.
Especially, to my children, who educate me and inspire me on a daily basis.

Acknowledgements

I have been very fortunate to be given help to be and achieve what I have today. So, I would like to acknowledge:

Professor J. W. Morris Jr., Chris Kinney Ph.D. and Kyu-Oh Lee Ph.D. – Research collaborators and mentors.

Intel Corporation for funding this research.

The University of California for their Grants and Dissertation Year Fellowship.

The Zachary Michael Cruz Foundation.

The Foster City Rotary Club.

Diana Lizarraga and the UC Berkeley NERDS Program.

The MSE Dept. Faculty and Staff.

Your support was key in the completion of this work.

It took a village to get me here. So, I would also like to thank the individuals that believed in my potential and offered me a helping hand along the way.

Thank you!

Table of Contents

Chapter 1: Introduction 1
Motivation 1
Objective 1
Methodology 1
Chapter 2: Background 2
Lead-Based Solders 2
SnAgCu (SAC) Alloys 3
Sn-Cu Intermetallic Compounds 4
Electromigration 4
Literature Review 6
Chapter 3: Experimental Procedures 7
Sample Preparation 7
Characterization Techniques 8
Orientation Imaging of EBSD data 8
Phase Identification of EBSD data 11
Quantitative Techniques 11
Chapter 4: Results 13
Effect of Orientation on Electromigration 13
Effect of Microstructure on Electromigration 16
Effect of Ni barriers on solder joints 17
Incubation Period for Electromigration 21
Intermetallic Growth Curves 21
Single Crystalline Samples 23
Polycrystalline Samples 25
Chapter 5: Discussion 26
Electromigration Equation 26
Chapter 6: Conclusion 31
References: 32

Chapter 1: Introduction

Motivation

In the past decade, there has been a lot of concern over the large amounts of electronic waste created and its disposal. Some electronic devices contain hazardous materials such as lead. These devices are sometimes disposed of in landfills where their toxic materials can leak out and contaminate the water stream and later people. Lead consumption, specifically, affects the nervous system and can cause brain and kidney damage that lead to death. In order to reduce the amount of hazardous materials from electronics and recycle e-waste, policies, such as the Restriction of Hazardous Substances Directive (RoHS), were put into effect to eliminate the use of lead and other hazardous materials in electronics. This directive aims to restrict the use of several hazardous substances in electronics, including lead, mercury, and cadmium (among others). The directive is a complement to the Waste Electrical and Electronic Equipment (WEEE) Directive, which is part of a legislative initiative to address the large amount of toxic electronic waste (e-waste) [1].

As a result, the lead based solders used to build printed circuit boards (PCBs) and Integrated Circuits (ICs) have had to be replaced by lead free solder interconnects. However, the transition has been difficult as there has not enough reliability data on lead-free solders to accurately predict the life time of the new devices. In addition, the miniaturization of ICs, and consequently solder joints, has made them susceptible to electromigration damage, which poses a major reliability challenge and has not been fully understood.

Objective

The main goal of this research is to help assess the reliability of new electronic devices by studying electromigration phenomena in new lead free solder joints. More specifically, to quantify electromigration in lead free solder systems and identify conditions that may improve the reliability of electronic materials. Although research has been done on the electromigration of lead free solders, there has been little progress on the quantitative analysis of it because of the complex processes that occur with electromigration. So, researchers have agreed to research the individual processes that occur during electromigration in order to get the pertinent parameters and be able to have a quantitative analysis of electromigration. As a result, this study uses idealized interconnects to measure electromigration and through that, quantify the effective charge (z^*) of Cu in the Sn-Ag-Cu alloy SAC 305, which is made of 3% Silver, 0.5% Copper and 96.5% Sn.

Methodology

The emergence of Sn-Ag-Cu solders as leading candidates to replace leaded solders has led to a considerable body of work on their microstructure and properties. A significant part of this work has focused on the electromigration behavior of these solders. Electromigration is a directional diffusion phenomena caused by an imposed current [2-8]. The imposed current creates a net migration of atoms, including copper, due to an 'electron wind', and can accelerate the growth of various intermetallic compounds (IMCs), most notably Cu_6Sn_5 [9,10]. The driving

force for electromigration, the effective charge, z*, is a dimensionless measure of the electrostatic and 'electron wind' forces on an atom, of which the 'electron wind' force is dominant [11-13]. β-Sn which comprises the bulk of the interconnect, has a tetragonal structure. Therefore, the properties of β-Sn, particularly including the diffusivity of solute Cu [12,14,15], change with the orientation of the tetragonal axis: the [001] c-axis [3,16-18]. As solder interconnects are made smaller, they are more likely to be composed of a single grain of Sn. Given anisotropy, electromigration damage may occur at an accelerated rate in single-crystalline Sn with unfavorable orientation, leading to premature failure. For this reason this study examined the effect of the Sn orientation on electromigration.

Investigations regarding the orientation of Sn have greatly benefited from the use of electron backscatter diffraction (EBSD) techniques [3,16,17]. EBSD methods allow grain orientations to be mapped quickly over large areas. These techniques were employed in this study to map the orientations of the grains before and after electromigration in order to determine the effect of Sn crystal orientation on its response.

To successfully undertake this study, idealized samples were used to be able to neglect the complex interactions present in standard microelectronic packages. Typically, these interactions include complex current flow patterns and thermal profiles. The simplified sample configuration allows us to study the influence of current on mass flow and IMC growth without having to separate out thermal gradient, stress or "current crowding" effects [4,5]. In particular, the simple sample geometry facilitates measurements of the magnitude and orientation dependence of the effective charge (z*) for Cu electromigration in Sn.

Chapter 2: Background

Lead-Based Solders

Lead based solders have been used for decades to connect electrical components together. Printed circuit boards (PCBs) and Integrated Circuits (ICs) were some of the applications that were built using solder made of 63Sn-37Pb (eutectic composition) or 60Sn-40Pb (near-eutectic composition). The Sn-Pb solder system yields soldering conditions compatible with most electronic materials and devices. The system has suitable mechanical, thermal, electrical, and chemical properties with a low eutectic melting temperature of ~183 °C , ideal properties for manufacturing purposes [19]. Having lead as the primary component in eutectic solders brings many advantages. One of them, is that it reduces the surface tension of pure tin, and that of the solder, resulting in better wetting properties [20]. The wetting ability of a solder system is very important since the molten solder needs to adhere to the substrate material in order to bond to it and create an electrical connection. Also, the presence of a Pb impurity, as minimal as 0.1 wt. %, can prevent the thermodynamic transformation of β-Sn to α-Sn when the system is cooled past 13 °C. This is favorable because this crystallographic transformation result in a 26% volume increase and causes the Sn and solder to lose its structural integrity [21]. Another advantage is that it serves as a solvent metal allowing other alloying elements (e.g. Sn, Cu) to quickly form intermetallic bonds by diffusing in the liquid state [19]. In addition, Pb is readily available and inexpensive. For these reasons, Pb is an ideal element to alloy with Sn and lead based solders were the preferred electrical connecting material in the past.

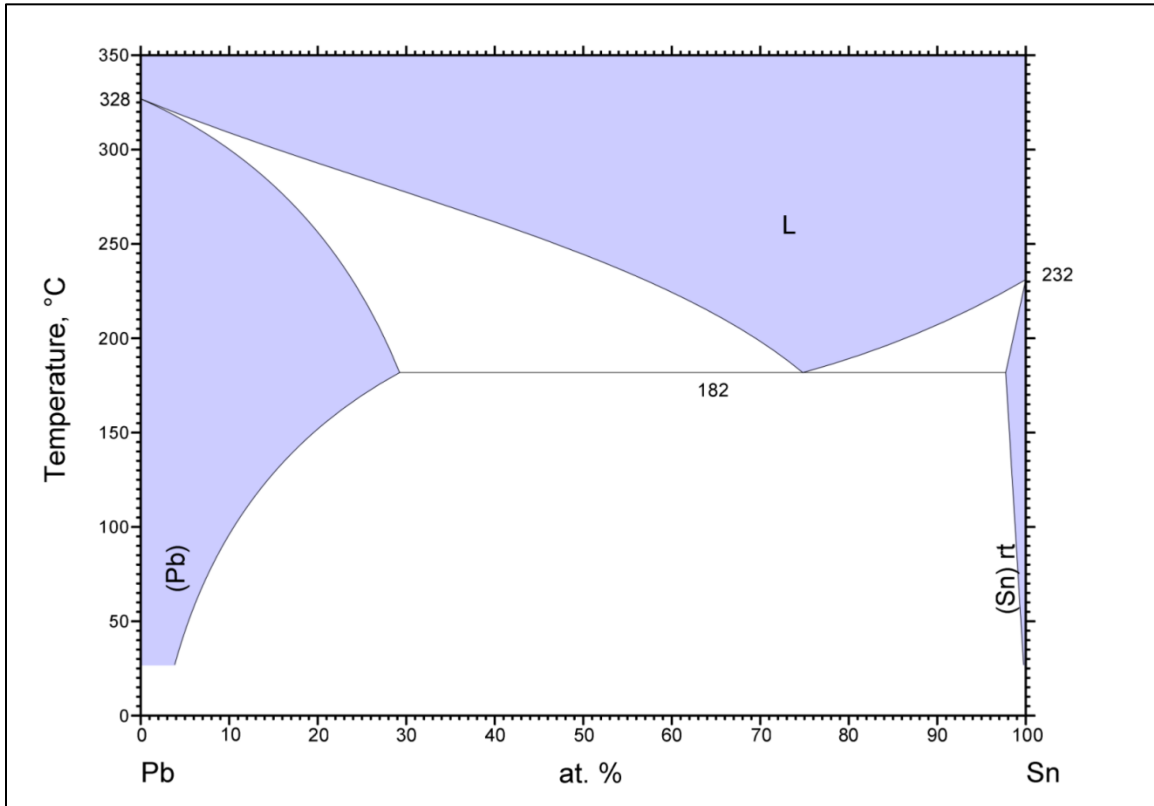

Figure 1: Pb-Sn Binary Phase Diagram [22]

SnAgCu (SAC) Alloys

The SAC system has been highly regarded as the leading replacement for lead-based solders. Its relatively low melting temperature (in comparison to the Sn-Ag eutectic), superior mechanical properties, acceptable wetting properties, and a generally good compatibility with the electrical components have given SAC alloys the most potential for broad use in the electronics industry. SAC solders can promote enhanced joint strength, creep and thermal resistance, and have the ability to increase operating temperatures for the manufacture of more advanced electronics [23]. Because of the formation of small-dispersed particles, the SAC joints have fine and stable microstructures; this increases their shear strengths. However, SAC solders do require a higher reflow temperature, due to their higher melting point. This is a pitfall, as the higher melting temperature requires a new reflow profile, and raises concerns about the stability of components.

The SAC system has a ternary eutectic at Sn-3.5Ag-0.9Cu with a melting temperature of 217 °C. This eutectic composition is a favorable choice because it behaves as an independent homogenous phase, has a unique metallographic structure, and a distinct melting point. However, near eutectic Sn-3.0Ag-0.5Cu (SAC 305) has become the most popular composition for electronic applications since it has adequate silver concentration to enhance electrical properties while minimizing costs. Because of its vast implementation, this researched focused on studying electromigration in SAC305 solder joints.

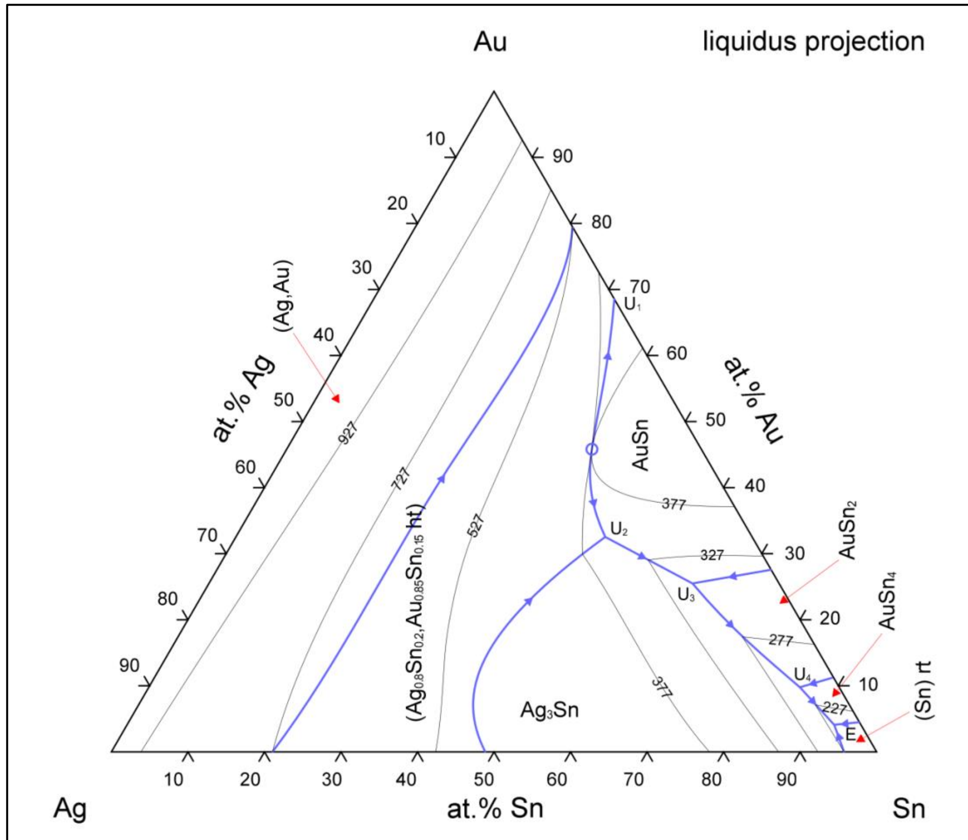

Figure 2: Ternary Phase Diagram for Sn-Ag-Cu (SAC) System [24]

Sn-Cu Intermetallic Compounds

Lead free solders made of near eutectic alloys, like SAC 305, are Sn rich with small amounts of additives. When joint to Cu surfaces, these solders create IMCs, Cu_3Sn, Cu_6Sn_5, and other IMCs depending on the content of the solder. For SAC 305, thin layers of Cu_3Sn and Cu_6Sn_5 are formed since Ag-Cu do not form intermetallics, and there isn't enough Ag to form Sn-Ag intermetallic, Ag_3Sn. These IMC layers that form in the interfaces between the molten solder and the Cu surfaces strengthen the bond between the jointed electrical components and decrease the stress concentration through the joint. However, Cu_3Sn and Cu_6Sn_5 are brittle compounds that can easily crack during thermal cycling or mechanical shock, thus threatening the reliability of the interconnects.

Electromigration

Electromigration is a phenomenon in which atoms migrate due to high imposed currents in conducting materials. The driving force for electromigration is momentum transfer from electrons to thermally activated atoms. The direct force and the wind force are those which oppose the net force that gets exerted on a metal ion in a conductor undergoing electromigration. The direct force comes about through the application of an electric field, which exerts an

electrostatic pull on the core of the metal ion. This can be described quantitatively in the following equation where a is the screening factor (a<<1), Z is the actual valence of the atom, e is the electron charge (1.6 x 10^{-19} C), j is the current density in units of A m^{-2}, and ρ is the resistivity in units of Ω m.

$$F_d = aZeE = aZej\rho \quad (1)$$

Originally it was thought that the flow of metal ions during electromigration would follow the convention in electrolysis, that electrons would flow toward the cathode; this is true sometimes, however for ICs, migration most often flows toward the anode instead. This behavior can be attributed to the wind force, which overpowers the direct force in IC applications. Wind force comes about as a result of changes in acceleration due to electron scattering within the crystal lattice, which occur due to imperfections in the crystal. This wind force is a function of electron density(n_e), collision cross-section (σ_i), and mean free path(λ) [2-8].

$$F_w = -en_e\lambda\sigma_i E \quad (2)$$

Therefore, the net force of the metal ion cores which results in their atomic electromigration can be described as the sum of the wind and direct forces, where Z_{wind}, Z_{direct} and Z^* is the effective charge (valences) for the wind, direct, and net forces respectively[2-7].

$$F_{net} = F_{wind} + F_{direct} = (Z_w + Z_d)\, ej\rho = Z^* ej\rho \quad (3)$$

The outcome of this directional atomic diffusion is that hillocks form on the anode side of the joint and vacancies result on the cathode side. Therefore, it follows that the flux of atoms must be studied in order to understand these phenomena in the specific system under study.

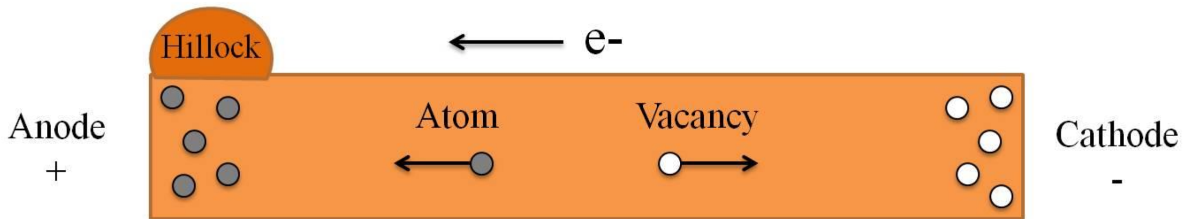

Figure 3: Electromigration in metals

In considering Sn-rich solder interconnects, it must be taken into consideration that solder joints are more complex systems, as they have different conducting materials in contact with one another. For a SAC 305 solder connecting two Cu pads, the reflow process creates small layers of Cu_3Sn and Cu_6Sn_5 at the interface between the Cu and the solder. During electromigration Cu atoms diffuse interstitially into the solder and accumulate at the boundary of the anode and the solder, thus growing the intermetallic compounds (IMC) [9-10]. Typically, on the anode side of the interconnect, a thin layer of Cu_3Sn remains and the Cu_6Sn_5 layer grows with time. On the cathode side of the interconnect, the initial (reflow-formed) IMC dissolves, as described later in Chapter 5.

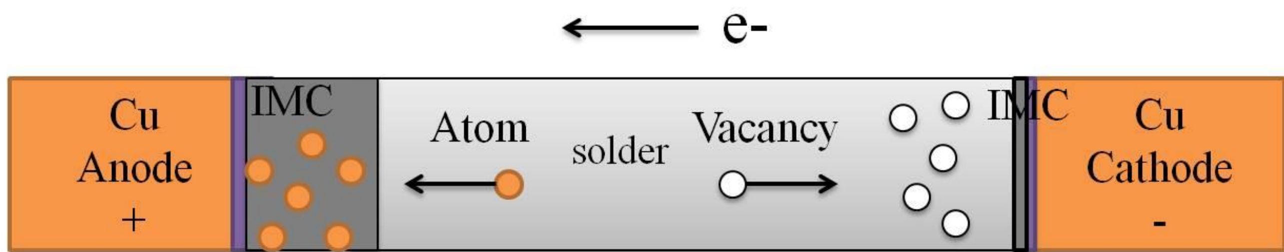

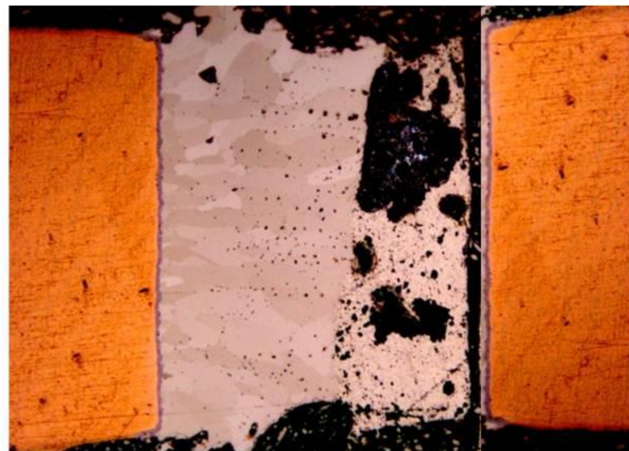

Figure 4: Eletromigrated Interconnect

Literature Review

Quantitative analysis of electromigration of the Cu in Sn system has not yet been determined, as one of the key parameters that contribute to electromigration has been missing. Researchers had tried to get z* in the past, but have not been successful, as the systems they tested were complex, with other migration processes occurring simultaneously. Most relevant efforts to quantify effective charge of Cu in various systems can be summarized in the table below. For these reasons, idealized samples were employed to simplify electromigration, in order to quantify the effective charge, and thus quantitatively analyze electromigration.

Table 1: Effective Charge of Cu

Species	Phase	Z*	Reference
Cu	Cu	2 - 7	[25-27]
	Sn (Pb)	0.6 - 3.25	[28]
	Cu_3Sn	26.5	[29]
	Cu_6Sn_5	26	[29]

Chapter 3: Experimental Procedures

Sample Preparation

The solder joints tested in this study were composed of a Sn-Ag-Cu alloy of Sn-3.0Ag-0.5Cu wt.% (SAC 305). A schematic of the samples employed in this study is given in Figure 5. To construct these specimens, Cu blocks were cut to dimensions of 11mm x 13mm x 6mm, and their broad faces were polished to 4000 grit. For single crystalline samples, the polished faces of the blocks were coated with flux and matched together while separated by 250µm spacers. The composite block was placed in molten Sn-Ag-Cu at 360°C for 45 seconds, then removed and cooled in air. Polycrystalline samples were made by placing the composite block in molten SAC 305 at 360°C for 45 seconds as well, but was quenched in water instead. To produce samples with a Ni layer, one Cu block was coated with a 10µm Ni layer and paired with a plain Cu block, both of which were coated with flux and separated by a 250µm spacer before being fastened together. The composite block was placed in molten SAC 305 at 360°C for 45 seconds, and air cooled (for single crystalline samples) or quenched in water (for polycrystalline samples). Once cooled, all blocks were polished to examine the quality of the solder joints, and then cut into sheets of roughly 500µm in thickness. These sheets were then polished with various slurries and suspensions to produce a damage free surface suitable for EBSD examination.

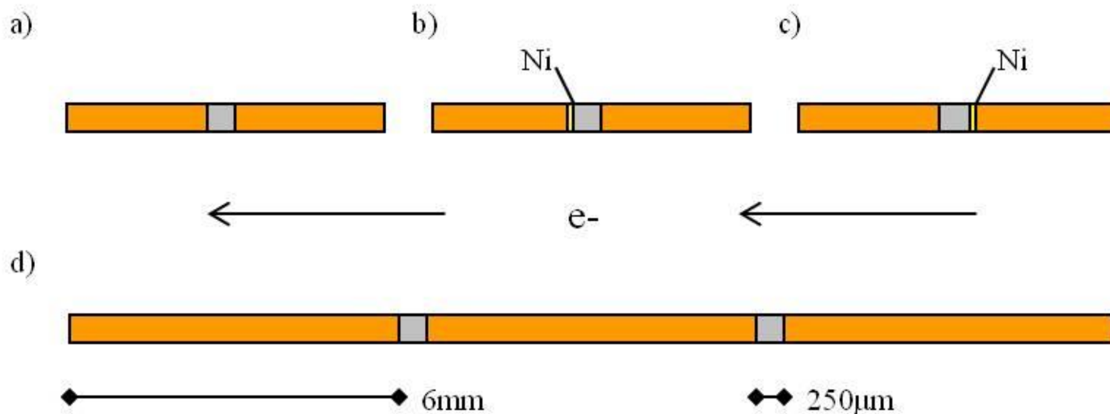

Figure 5: A schematic of the sample configuration; (a-c) are single jointed samples: (a) has no Ni layer, (b) Ni layer at the anode and (c) Ni layer at the cathode. (d) is a double joint sample.

The crystallographic orientation of the sheets was determined by a ZEISS SEM with an EDAX-TSL EBSD detector. Sheets were classified either as essentially single crystal with a particular crystal orientation or as polycrystalline. The specific single crystal orientations desired were ones with the c-axis parallel or perpendicular to the electron flow. The polycrystalline samples chosen were those that were sufficiently fine-grained that grains of many orientations were present in the cross-section. The sheets were then sectioned into rods. The rods were single- or double-jointed samples with square cross-sections, approximately 400µm x

400μm, and lengths of roughly 12.5mm (single joint) or 18.5mm (double joint). This sample configuration was designed, and has previously been used, to produce interconnects that have a constant cross section, but with a microstructures similar to that of BGA solder balls found in actual microelectronic packages [2-5].
The rod samples were placed in a current stressing apparatus and put into an oven. They were tested at either 10,000 A/cm^2 or 11,500 A/cm^2 for selected periods of time. Previous work using IR imaging, computer modeling and thermocouple measurements showed that this sample configuration maintains an even thermal profile across the solder joint [4]. The measured steady-state temperature was ~ 150ºC at a current density of 10,000 A/cm^2 and ~ 160ºC for 11,500 A/cm^2. Once samples were tested for the requisite amount of time, they were removed and placed into an epoxy-based metallographic mount, polished, and then re-examined by EBSD to determine the morphology of the interconnect after current stressing. TSL OIM Analysis software was used to create the various EBSD maps, as well as to measure the thickness of the Cu_6Sn_5 intermetallic layer present.

Characterization Techniques

Orientation Imaging of EBSD data

EBSD results can best be displayed in different forms. Figure 6 shows a 'typical' EBSD map of a single crystal sample, where a color coded map combined with an Inverse Pole Figure (IPF) key informs the viewer of the crystallographic orientation. The color represents the crystallographic direction in the sample that is parallel to the observation direction, usually taken as the normal to the plane of the sample. In Figure 6 the map has a green color, and the IPF key indicates that this color corresponds to the [100] direction. On the lattice schematic, the [100] direction, indicated by the green arrow, is pointing almost directly out of the page.

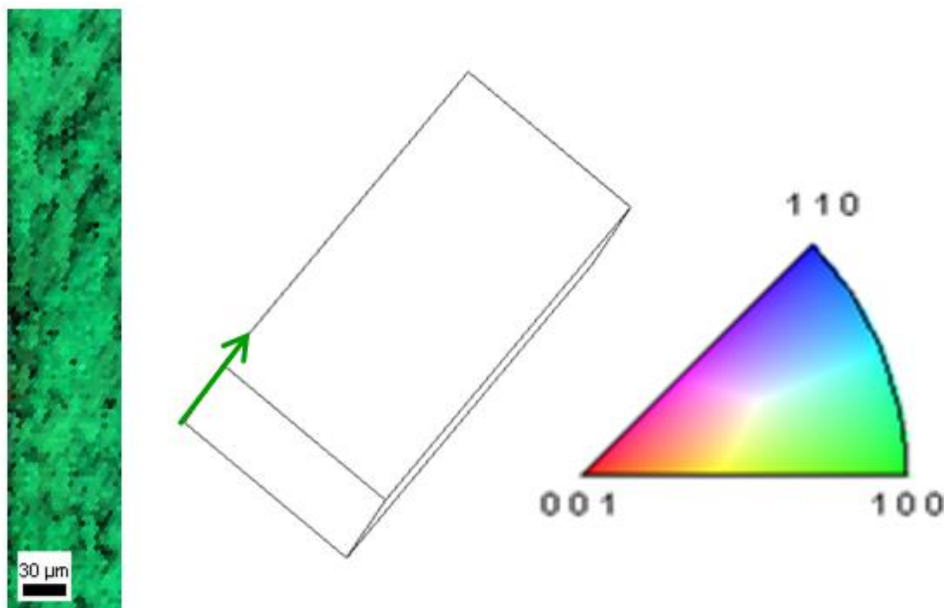

Figure 6: An EBSD map of a single crystalline sample, accompanied an IPF key. The green color corresponds to the [100]; the [100] direction is pointing almost directly out of the page.

However, this study is not concerned with the orientation relative to the sample normal. Rather, it is concerned with the relationship between the c-axis and electron flow. Therefore, it is more useful to view the EBSD results in a manner that directly displays the orientation between the c-axis and electron flow, like a crystal direction map. Figure 7 shows a schematic of such a configuration, where the color coding on the map denotes the angle between the c-axis and the electron flow. For the purposes of this study, grains with the same angle of deviation ($\theta_1 = \theta_2$) are given the same label. Note that when the c-axis is parallel to electron flow the color is blue, when the c-axis is perpendicular to electron flow, the color is red. For the IMC Cu_6Sn_5, the color coding is based on the angle relationship between the basal direction and electron flow.

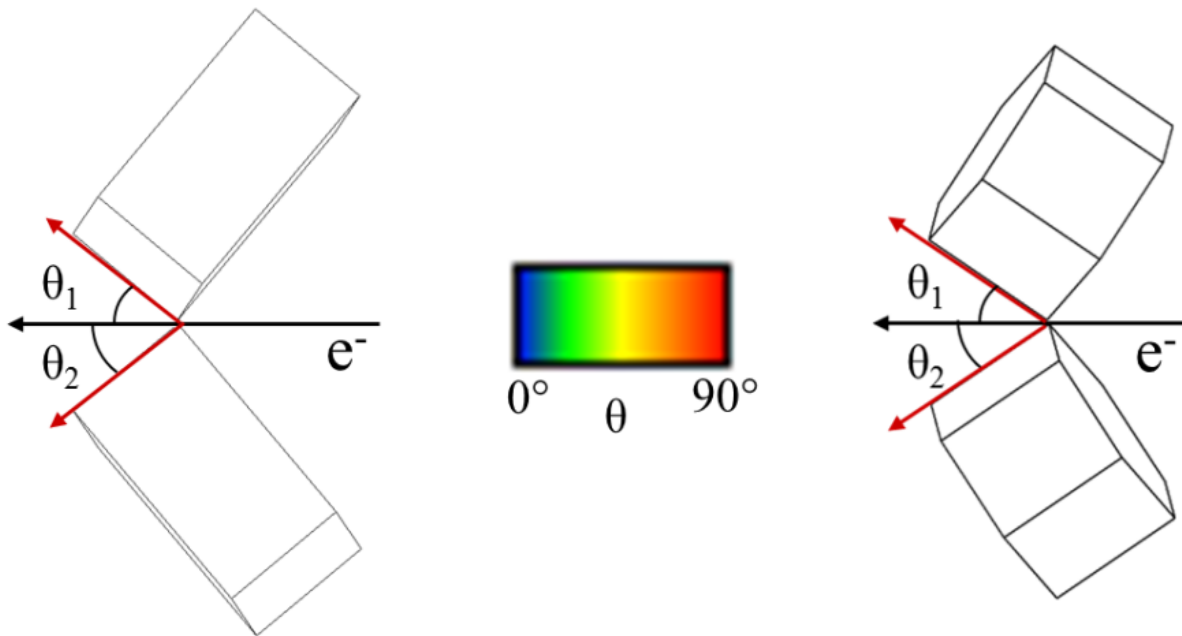

Figure 7: Schematic of a color code to show the orientation relationship between the c-axis and electron flow (for Sn) and between basal direction and electron flow (for Cu6Sn5) in EBSD maps.

Figures 8 and 9 show the benefits of this EBSD imaging method. In these figures, six samples are shown after being tested in an oven at 100°C (150ºC steady-state test temperature) under an imposed current of 10,000 A/cm^2; the electron flow is from right to left. The samples on the top row (a-c) all show characteristic Cu_6Sn_5 growth, moving from the anode into the solder joint. The samples in the bottom row (d-f) have no Cu_6Sn_5 growth visible. In Figure 8 these results are displayed in the 'typical' IPF map. In these images, it appears that samples b) and c) both have the [110] direction normal to the page, and both show IMC growth. Samples e) and f) both have the [001] direction normal to the page, and show no IMC growth. However, samples a) and d) are puzzling if not contradictory. They both have an orientation corresponding to the 'purple' direction; but sample a) shows Cu_6Sn_5 growth while there is no visible IMC growth in sample d).

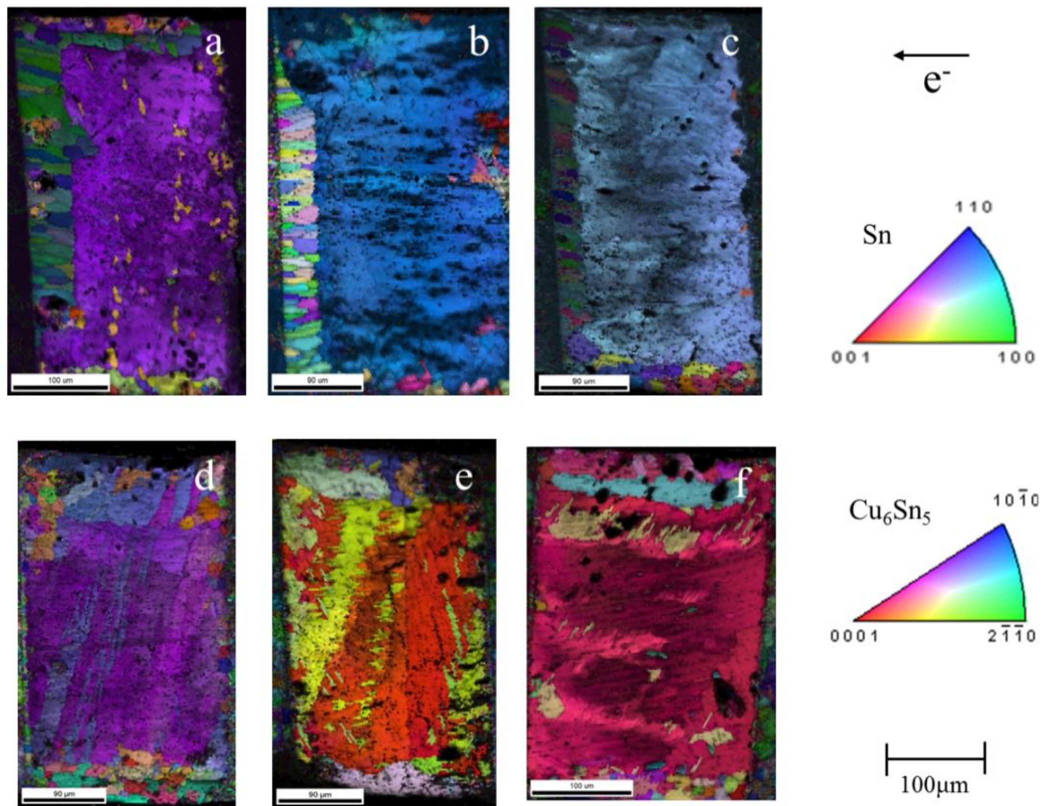

Figure 8: Samples tested at 100°C with 10,000 A/cm2, results presented in 'typical' IPF maps.

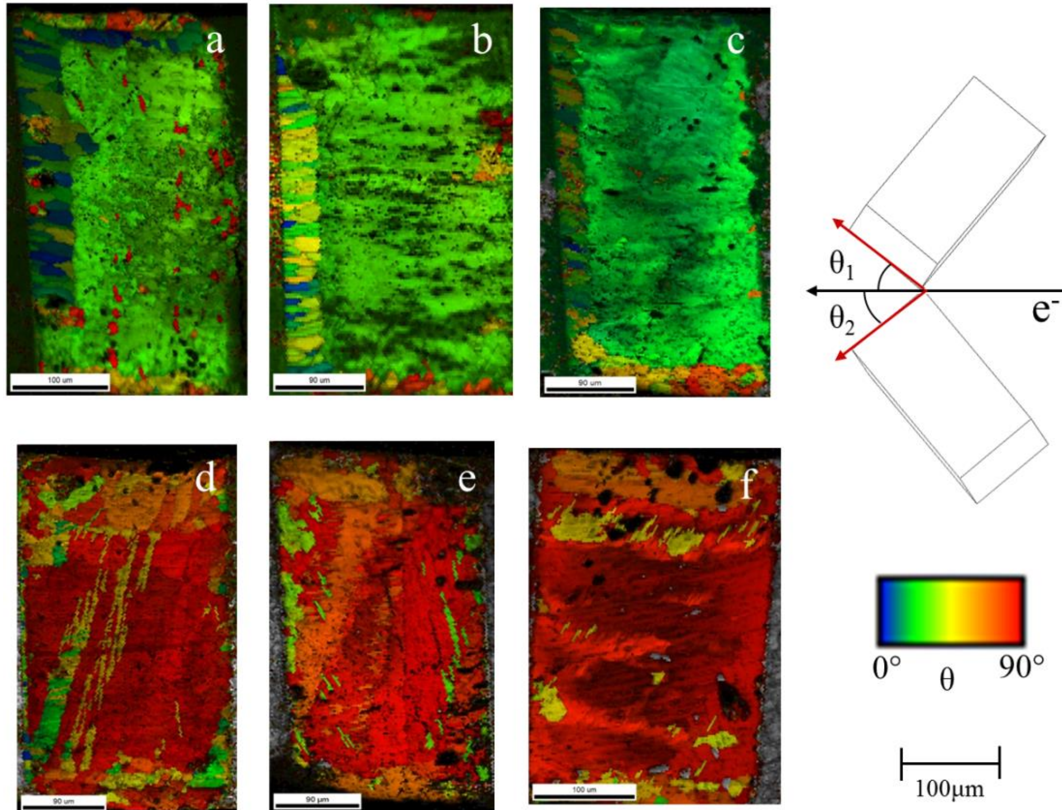

Figure 9: The same samples shown in Fig 4, this time presented using the θ-map color gradient in a crystal direction map.

When these same results are viewed in terms of the θ-map described above, they have the straightforward interpretation shown in Figure 9. For the top row of samples (a-c), the Sn c-axis is almost parallel to the electron flow, and all of these samples show significant Cu_6Sn_5 growth. For the bottom row of samples (d-f), the bulk Sn has its c-axis oriented perpendicular to the electron flow, and no Cu_6Sn_5 growth is visible. Comparing Figures 8 and 9, it is clear that viewing EBSD results using this θ-based coloration is more useful than the typical IPF map for current stressing investigations; all the results presented in this dissertation will use this θ-map representation.

After EBSD mapping the samples prior to testing, we found that certain crystal orientations appeared with great frequency, while others were rarely seen. For example, it was common to find single crystal interconnects with the c-axis perpendicular to the electron flow (red), but it was rare to find single crystalline interconnects with the c-axis exactly parallel to the electron flow (blue). At this time we do not have a good explanation for the scarcity of "blue" crystals. However, there were numerous single crystal joints with a green color, with the c-axis slightly tilted from the direction of the electron flow. Since the physical effect of the misorientation should vary with the cosine of θ, and cos(θ) is close to 1 for low values of θ (cos 15° = 0.97), these green-oriented samples can be considered to be "almost blue", with c-axes almost parallel to the electron flow.

Phase Identification of EBSD data

To clearly observe the IMC evolution during electromigration, this study also uses phase identification maps. They show tin rich areas in blue, Cu_3Sn in yellow, Cu_6Sn_5 in red and copper in green. Presenting our data in orientation maps and their corresponding phase maps highlights the correlations between grain orientation and IMC growth, and facilitates evaluating more complex samples such as polycrystalline interconnects.

Quantitative Techniques

Once the desired sample orientation is obtained and tested, growth timelines for the IMC in the joint can be created. The growth rate of the IMC on the anode side of the joint is determined by the rate of delivery of Cu through the solder to the growing interface. Since Cu can diffuse due to a concentration gradient and electromigration, it is necessary to know the contribution of both to the IMC growth. The equations below quantify the atomic flux of Cu into the solder; where C is the atomic density of Cu in Sn, D is the diffusivity of Cu in Sn, z* is the effective charge of electromigration, e is the electron charge, ρ is the resistivity, and j is the current density through the solder joint.

$$J = J_{chem} + J_{em} \tag{4}$$

$$J = -D\frac{\partial C}{\partial x} + C\frac{D}{kT}z^{*}e\rho j \tag{5}$$

At sufficiently high current densities the electromigration should dominate, in which case there will be no significant concentration gradient through the body of the solder. To test whether

electromigration dominates in the test conditions Wavelength Dispersive X-ray Spectroscopy was used to profile the Cu concentration through the joint. The results show a nearly constant Cu concentration within the joints. So the growth rate is fully determined by the electromigration flux of Cu to the growing interface.

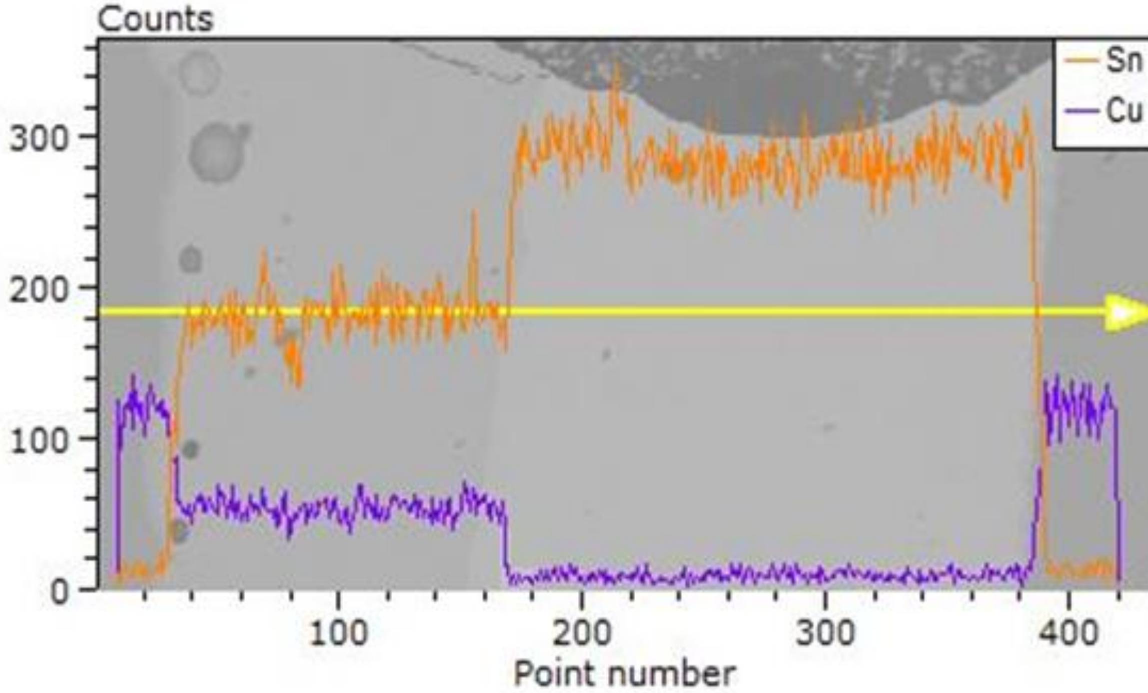

Figure 10: Copper concentration through the solder interconnect

The atomic flux of Cu can be found through the growth rate of IMC and the increase in the intermetallic layer per Cu atom. The growth rate is measured, and the lattice structure of Cu_6Sn_5 is used to know the volume increase associated with a single Cu atom. $\delta v = 3.24\text{x}10^{-29}$ m^3/atom. From there the electromigration equation is used to solve for the effective charge. More detailed derivations can be found in Chapter 5.

$$J^{EM}_{Cu,Sn} = \frac{dx}{dt}_{IMC} * \frac{Cu_atoms}{Volume_{IMC}} \tag{6}$$

$$J^{EM}_{Cu,Sn} = C\frac{D}{kT}z^{*}e\rho j \tag{7}$$

$$z^{*} = \frac{\frac{dx}{dt}_{IMC} * \frac{Cu_atoms}{Volume_{IMC}}}{C\frac{D}{kT}e\rho j} \tag{8}$$

Chapter 4: Results

Effect of Orientation on Electromigration

The results of testing both red and green oriented single crystalline samples at 100°C with 10,000A/cm^2 for 24, 48, 96 and 120 hours are shown in Figure 11. The top row of samples (a-d) were initially all "green" single crystals; the bottom row of samples (e-h) were initially all "red" single crystal. To clarify what part of the interconnect is IMC and what part remains Sn, the samples are re-shown Figure 12, but this time only the Cu_6Sn_5 is colored. It is clear from Figures 11 and 12 that the IMC grew steadily in the samples that had the c-axis parallel to electron flow (green) while there is no visible Cu_6Sn_5 growth in samples that had their c-axis perpendicular to electron flow (red). The red samples showed no IMC growth even after testing for 250h (We certainly expect that there is some IMC at the interface in the red samples. The point is that the growth rate is so slow that the IMC remains invisible at low magnification).

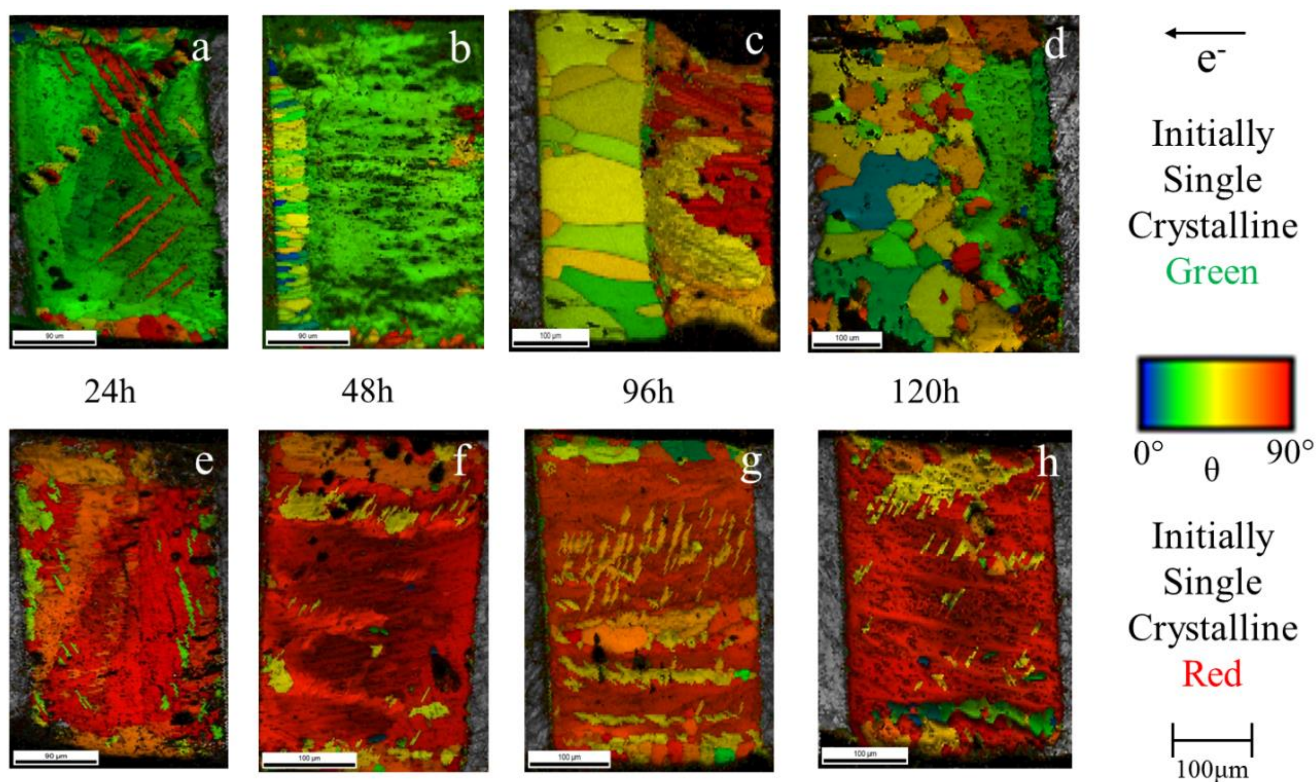

Figure 11: Samples tested at 100°C with 10,000A/cm2 for varying lengths of time. Samples (a-d) have the c-axis parallel to electron flow, whereas samples (e-h) had the c-axis perpendicular.

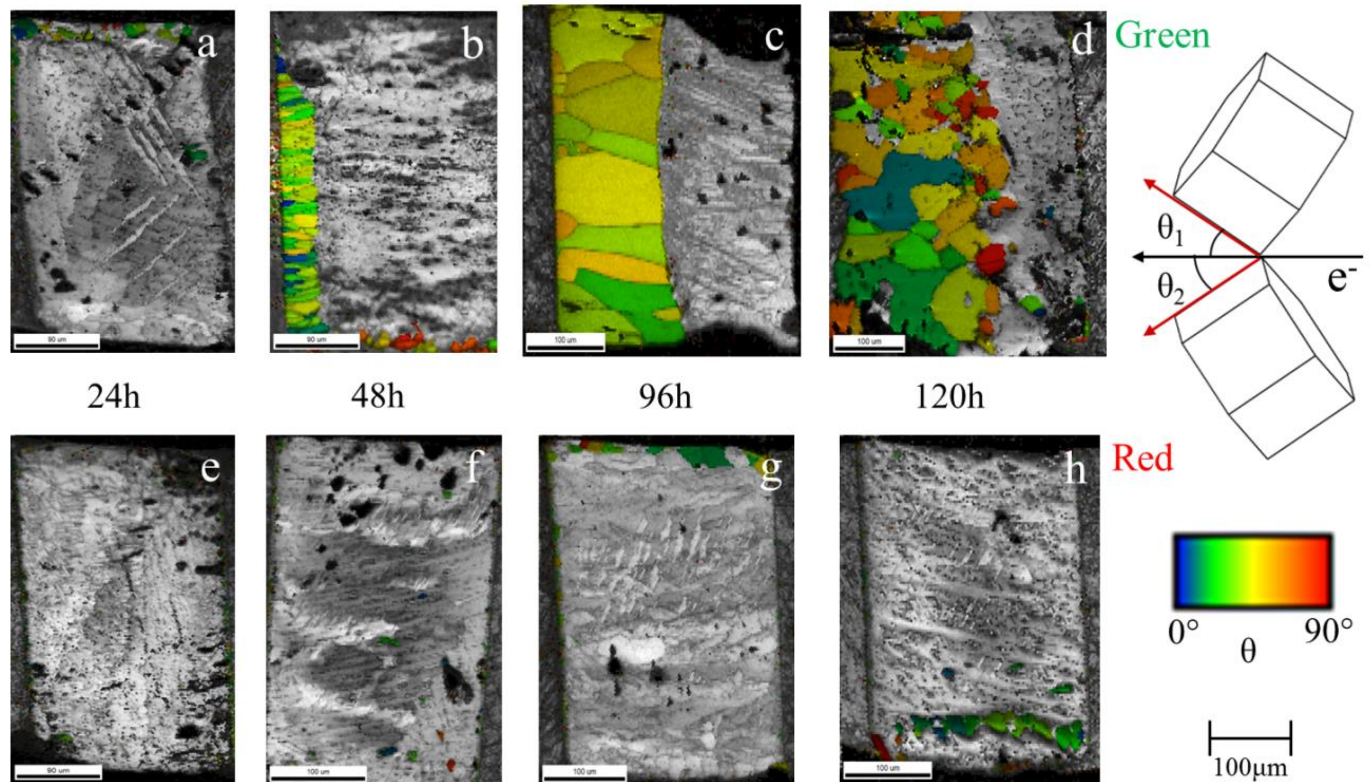

Figure 12: The same samples from Fig. 6, now with only the Cu6Sn5 colored. The difference in IMC growth between orientations with c-axis parallel vs. perpendicular to electron flow is clear.

The intermetallic layer grows either at the Cu-intermetallic interface at the substrate metallization, or at the intermetallic-Sn interface at the solder. Since the diffusion of interstitial Cu through Sn is known to be much faster than the diffusion of either Cu or Sn through the intermetallic, growth will be most rapid at the interface on the solder side, and the rate of growth should be determined by the rate at which Cu is delivered to the interface. Given the tetragonal crystal structure of Sn, however, the Cu diffusivity is anisotropic [12,14,15], which is the apparent reason the intermetallic growth rate is affected by the crystallographic orientation of the Sn.

The diffusivity of Cu in Sn was measured as function of orientation by Dyson et al [14]. We used their values for the pre-exponential factor, D_0, and the activation energy, E_a[14], to compute Cu diffusivities along the a-axis and the c-axis for the temperature used in this test. At the steady-state temperature in our tests at 10^4 A/cm^2, 150 ± 3ºC, the ratio of diffusivities is $D_c / D_a \sim 43$. It is, hence, unsurprising that the intermetallic layer grows at an appreciable rate along the Sn c-axis under conditions where there is a very low growth rate along the a-axis.

To obtain an observable growth rate along the Sn a-axis we increased the current density to 11,500A/cm^2, which raises the steady-state temperature to 160ºC. There is, hence, an increase in both the current stress and the Cu diffusivity ($D_c / D_a \sim 65$) to promote intermetallic growth. Figure 13 shows the results of tests done on single crystal joints at 11,500A/cm^2 and an ambient temperature of 100ºC (steady-state temperature of 160ºC at the joint). We have included images with both Sn and Cu_6Sn_5 colored (Figuare 13a,b) and images with just the Cu_6Sn_5 colored (Figure 13c,d) for visual clarity. The "red" sample (c-axis perpendicular to the current) that was

tested for 48 hours shows significant intermetallic growth. The thickness of the intermetallic layer is comparable to that obtained in a "green" sample (c-axis nearly parallel to the current) after testing for the shorter period of 6h (Figure 13b,d).

Interestingly, in most cases the growing intermetallic layer has a nearly planar interface with the solder, despite the columnar grain structure of the intermetallic. This morphology differs qualitatively from the rough, globular morphology of Cu_6Sn_5 intermetallic layers that develop after reflow, and suggests that the rate of intermetallic growth is determined almost entirely by the rate of delivery of Cu to the interface, irrespective of the local crystallographic orientation of the growing intermetallic.

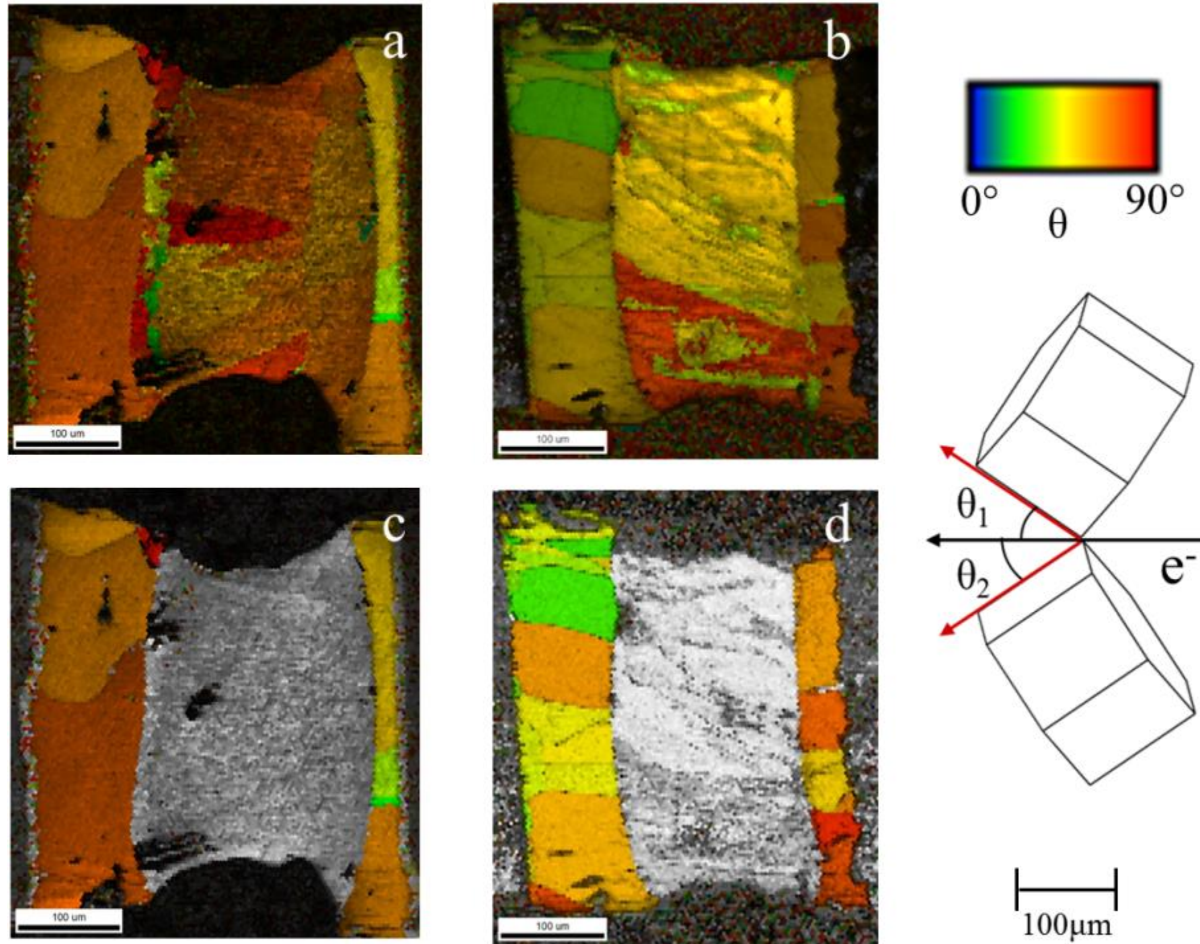

Figure 13: Samples tested at 100°C with a current density of 11,500 A/cm2 (160ºC steady-state temperature at the joint). Sample a) initially had a red orientation, and was tested for 48h. Sample b) initially had a green orientation, and was tested for 6h.

Given the planarity of the interface between the intermetallic and the solder it is possible to define the thickness of the layer with some meaningful accuracy and compute a growth rate. The measured layer thickness (x) is plotted as a function of time, crystallography and test condition in Figure 14. The data show that there is a significant incubation time for growth at the beginning of each test, after which the intermetallic layer thickens at an almost constant rate. The growth rates in the linear growth regime are:

$dx/dt = 2.3$ µm/hr ("green" orientation, 10^4 A/cm^2, 150ºC)
$dx/dt = 115$ µm/hr ("green" orientation, 1.15×10^4 A/cm^2, 160ºC)
$dx/dt = 11$ µm/hr ("red" orientation, 1.15×10^4 A/cm^2, 160ºC)

At the higher temperature and current density the intermetallic grows 10x as quickly in the "green" samples as in the "red" ones.

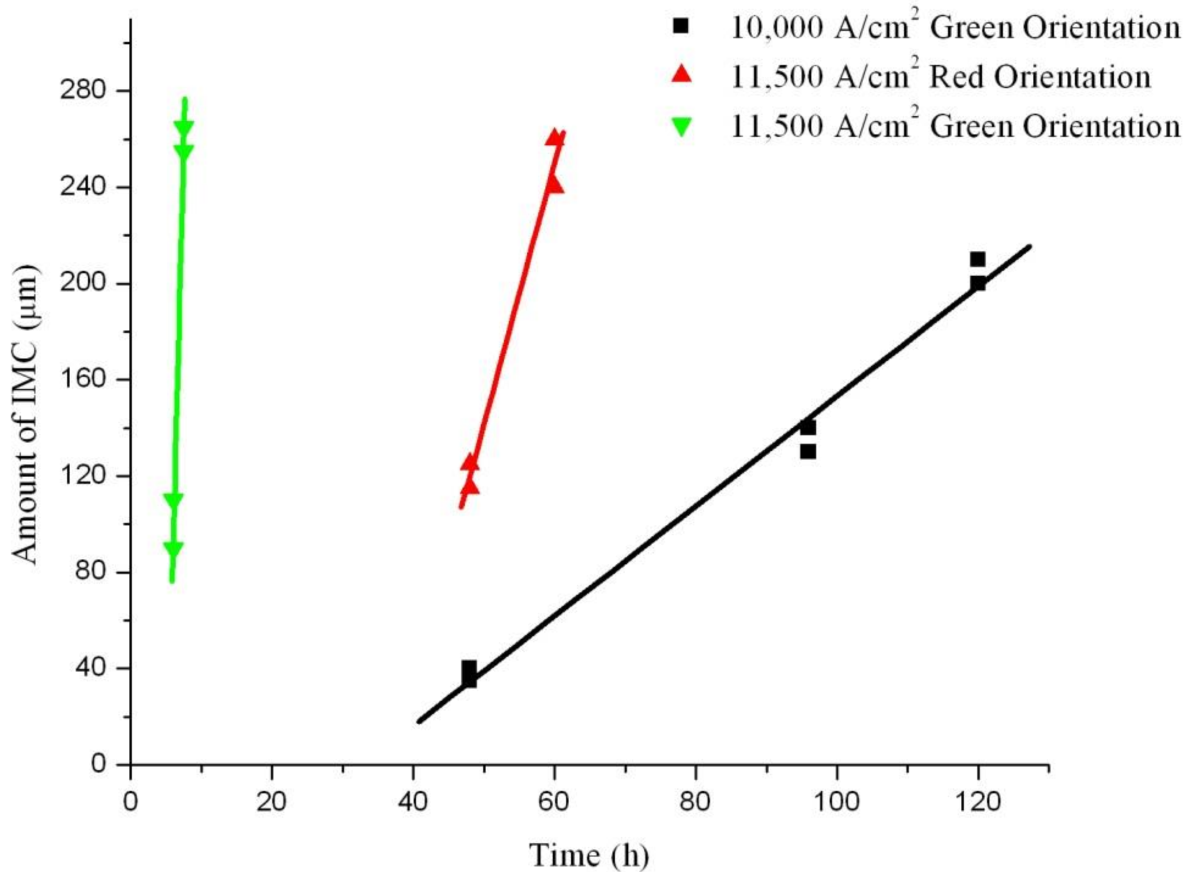

Figure 14: The measured thickness (x) of the intermetallic layer plotted as a function of time for the two crystal orientations and test conditions.

Effect of Microstructure on Electromigration

The results of tests done at 11,500 A/cm^2 for single crystalline “red” and “green” samples and polycrystalline samples are shown in Figure 15. The lower rate of intermetallic growth in the “red” samples is obvious. Moreover, there is a significant incubation time for growth at the beginning of each test, after which the IMC layer thickens at an almost constant rate. Interestingly, intermetallic growth in the polycrystalline samples is almost identical to that in the “red” single crystalline samples; following a long incubation period, the intermetallic thickness increases linearly with time at a rate almost identical to that of the “red” crystals.

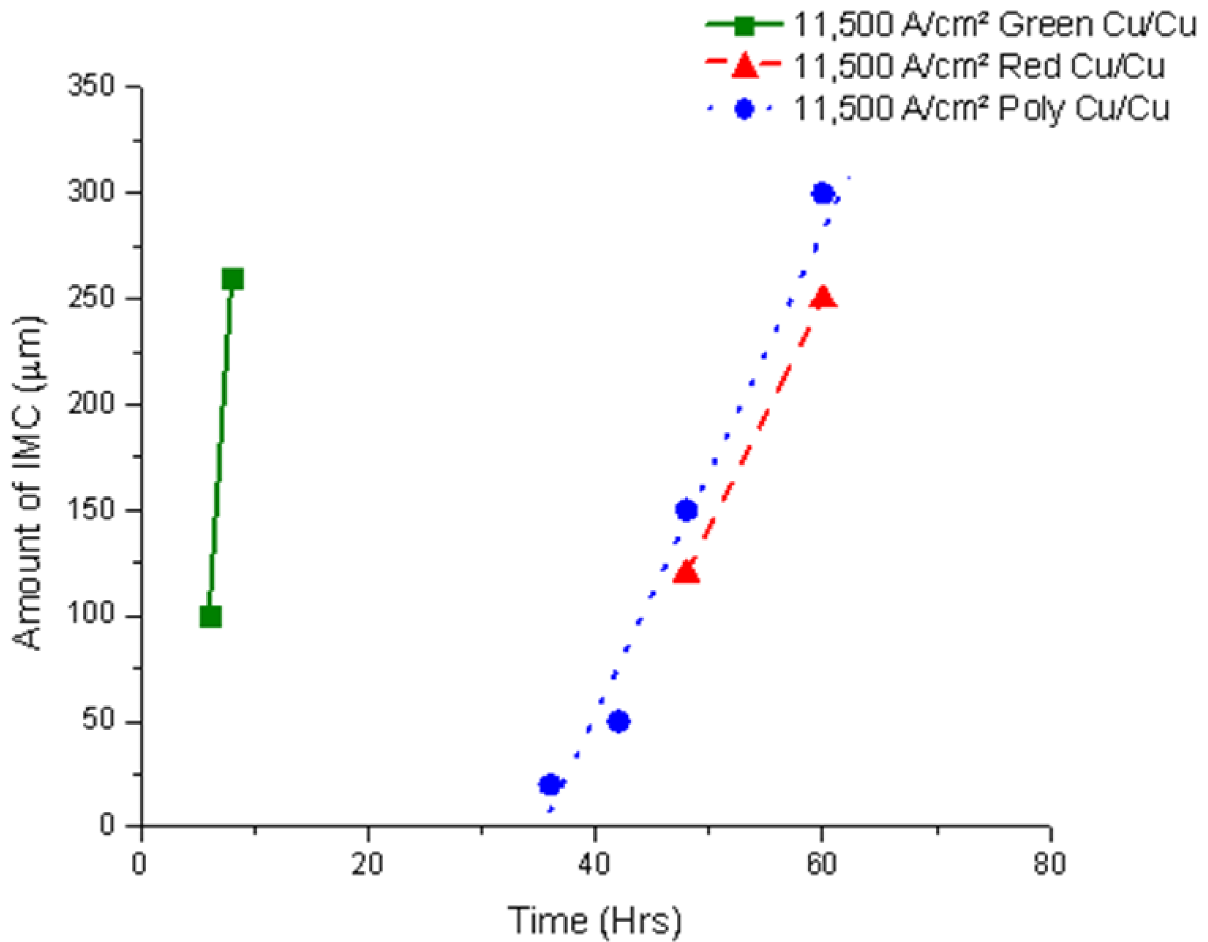

Figure 15: The measured thickness (x) of the intermetallic layer plotted as a function of time for both single crystalline and polycrystalline samples with no Ni layer, tested at 11,500A/cm^2.

Effect of Ni barriers on solder joints

When the Ni layer was placed on the anodic side of the interconnect, the Ni layer was effectively 'downstream' from the electron flow. As such, for both single and polycrystalline samples the anodic Ni layer had little effect on the rate of IMC growth, as shown in Figures 16-18. Note that the "green" samples in Figure 16 were tested at 10,000 A/cm^2, while the "red" and polycrystalline samples were tested at 11,500A/cm^2, for reasons discussed above. In Figure 17 one can see how similar the IMC growth rates are between the polycrystalline samples and the single crystal samples with the c-axis perpendicular to electron flow. Figure 18 shows the actual EBSD images for both the "red" and polycrystalline samples, and again, the growth rate of the IMC is similar in both. In all cases, the presence of a Ni layer at the anode had very little effect on the IMC growth rate.

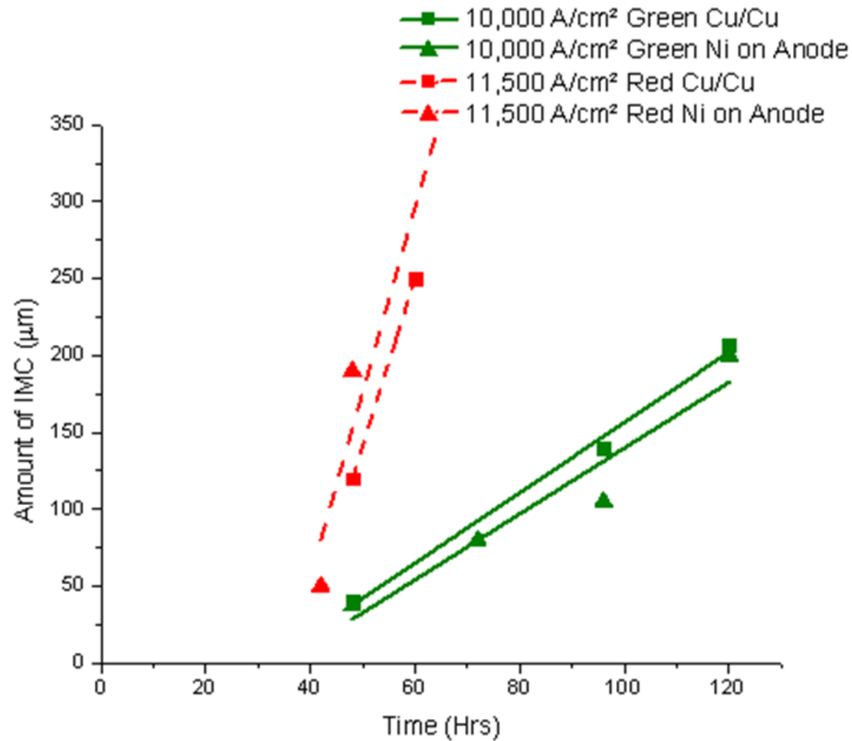

Figure 16: The measured thickness (x) of the intermetallic layer plotted as a function of time for both single crystalline samples with no Ni layer, and with an anodic Ni layer.

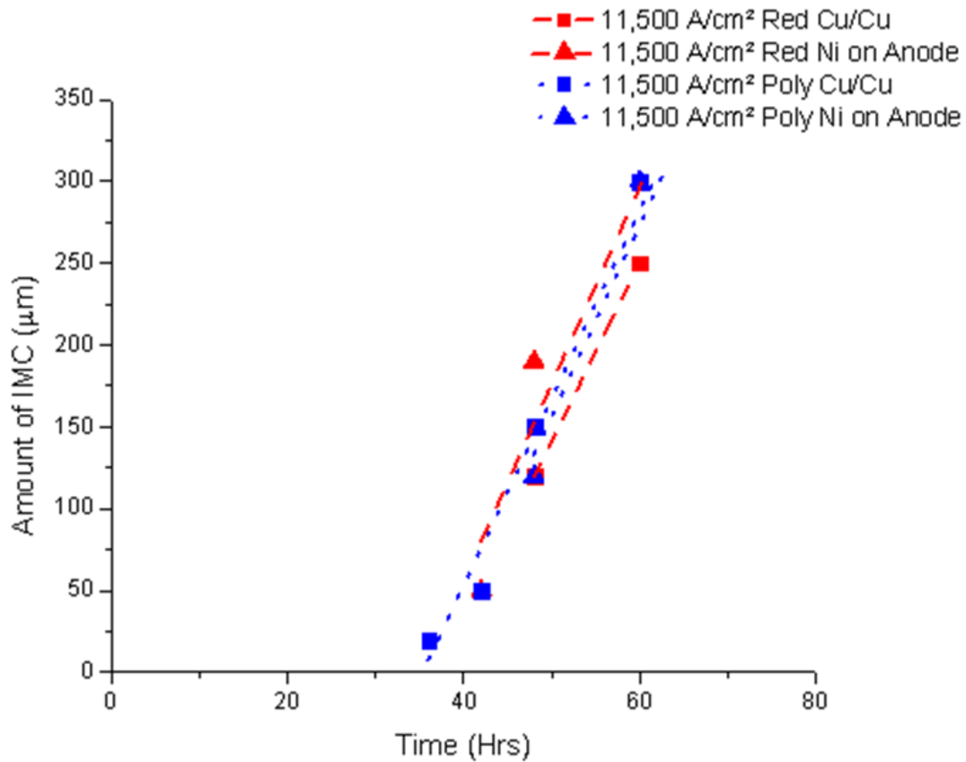

Figure 17: The measured thickness (x) of the intermetallic layer plotted as a function of time for "red" single crystalline and polycrystalline samples with no Ni layer, and with an anodic Ni layer.

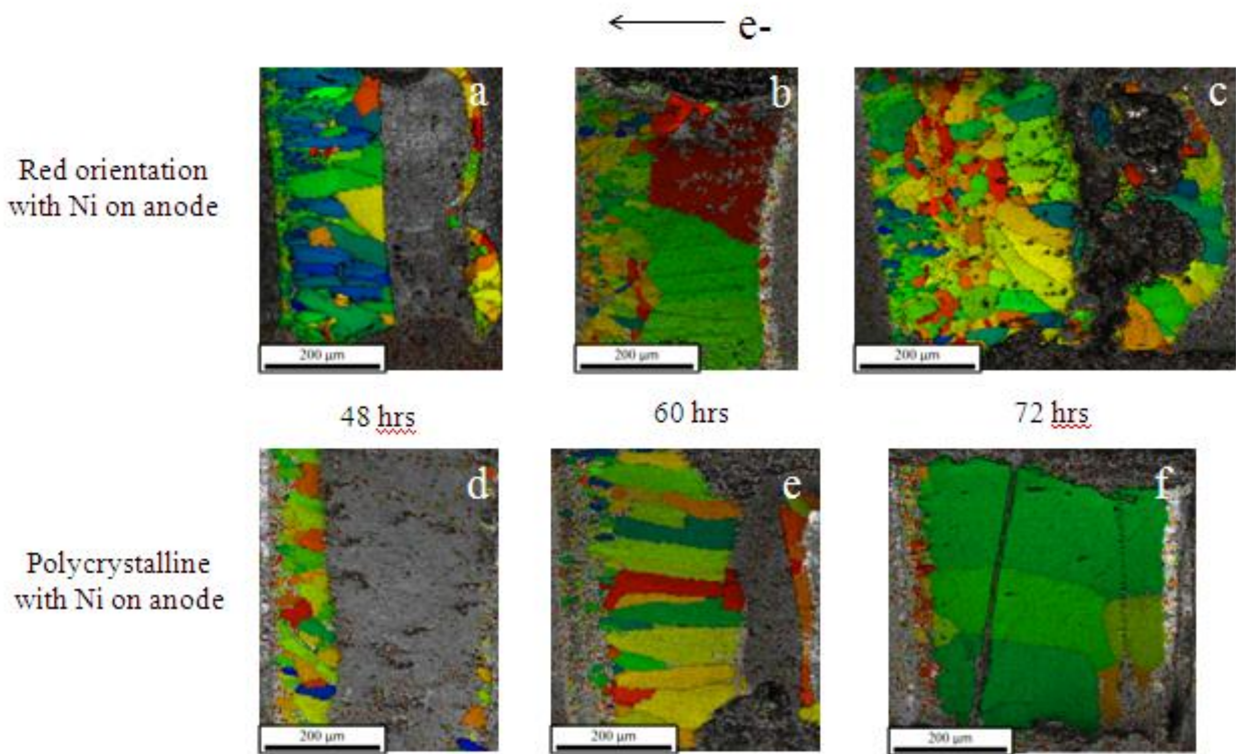

Figure 18: Samples tested at 11,500A/cm2 for varying lengths of time. Samples (a-c) are single crystalline with the c-axis perpendicular to electron flow, whereas samples (d-f) are polycrystalline. All samples (a-f) had a Ni layer on the anode.

However, when the Ni layer was placed on the cathodic side of the interconnect, there was a significant decrease in the IMC growth rate for all sample types. The effect of the Ni layer on the cathode side can be seen in Figures 19 and 20. Note that regardless of sample type, the rate of the IMC growth decreased; dramatically so for both the single crystal 'red' samples and the polycrystalline samples. The evident explanation for this behavior is that the cathodic Ni layer acts as a 'diffusion barrier' to Cu, slowing Cu diffusion into the bulk Sn [30]. Since less Cu is able to diffuse through the interconnect, the IMC grows at a slower rate compared to samples that have no Ni layer at the cathode. The IMC growth rates of all sample varieties are tabulated in Table 2.

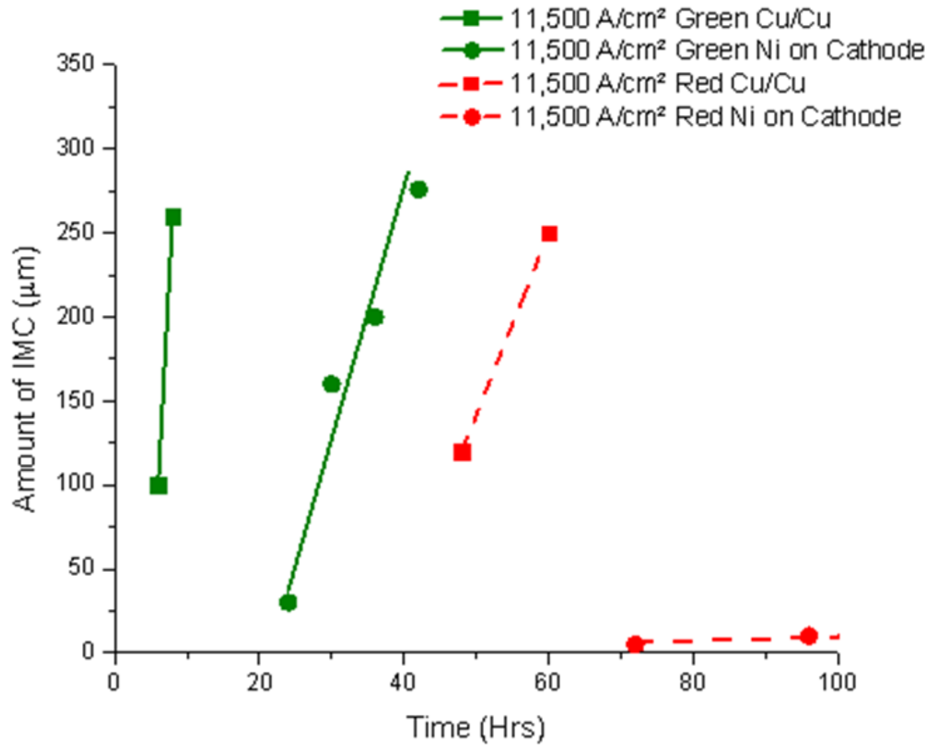

Figure 19: The measured thickness (x) of the intermetallic layer plotted as a function of time for both single crystalline samples with no Ni layer, and with a cathodic Ni layer.

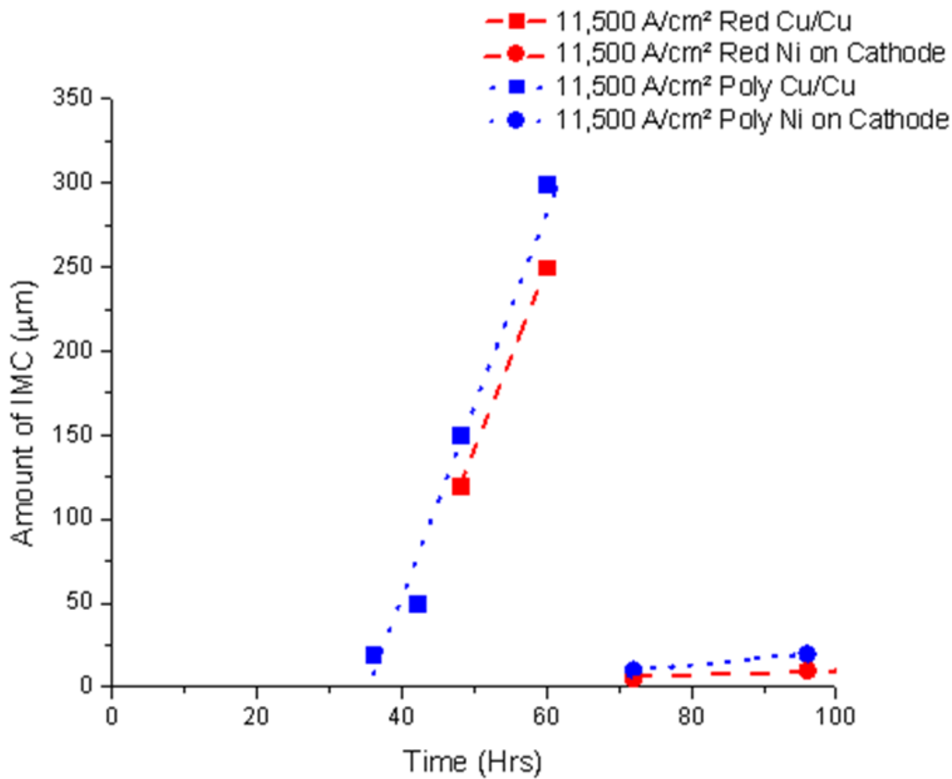

Figure 20: The measured thickness (x) of the intermetallic layer plotted as a function of time for "red" single crystalline and polycrystalline samples without Ni layer, and with a cathodic Ni layer.

Table 2: The growth rates of Cu_6Sn_5 for all sample conditions.

Specimen	dx/dt (µm/hr)
Green Orientation	
Cu/Cu, 10K A/cm², 150°C	2.3
Cu/Cu, 11.5K A/cm², 160°C	115
Ni on Anode, 10K A/cm², 150°C	2.1
Ni on Cathode, 11.5K A/cm², 160°C	15.0
Red Orientation	
Cu/Cu, 11.5K A/cm², 160°C	11.0
Ni on Anode, 11.5K A/cm², 160°C	12.0
Ni on Cathode, 11.5K A/cm², 160°C	0.1
Polycrystalline	
Cu/Cu, 11.5K A/cm², 160°C	11.4
Ni on Anode, 11.5K A/cm², 160°C	11.7
Ni on Cathode, 11.5K A/cm², 160°C	0.4

Incubation Period for Electromigration

Intermetallic Growth Curves

When interconnects are made, molten solder comes in contact with the two Cu surfaces it will connect and a small layer of IMC is formed at the interfaces between the Cu and the solder. During electromigration, the IMC layer on the anode side of the interconnect growths, and its growth is determined by the rate at which Cu is delivered to the interface. However, it seems that before the IMC layer can start growing, an incubation period takes place. From our previous results, IMC growth curves were created and a compilation of the results is shown Figure 21. The IMC timelines show an initial period of time where no IMC growth occurs in all samples regardless of their orientation or set up. This incubation period is longer for samples with their c-axis perpendicular to electron flow (red), polycrystalline, under lower current densities, and with a Ni layer on the cathode side of the interconnect.

The results of tests done at 11,500 A/cm^2 for single crystalline “red” and “green” samples and polycrystalline samples are shown in Figure 22. The fast diffusivity of Cu in “green” oriented Sn samples at 160ºC combined with the high current stress of 11,500A/cm^2 accelerated significantly its incubation period and intermetallic growth. The longer incubation period and lower rate of intermetallic growth in the “red” samples is understandable since “red” samples have a lower diffusivity. Moreover, polycrystalline samples show similar behavior to “red” single crystalline samples; following a long incubation period and having similar linear IMC growth.

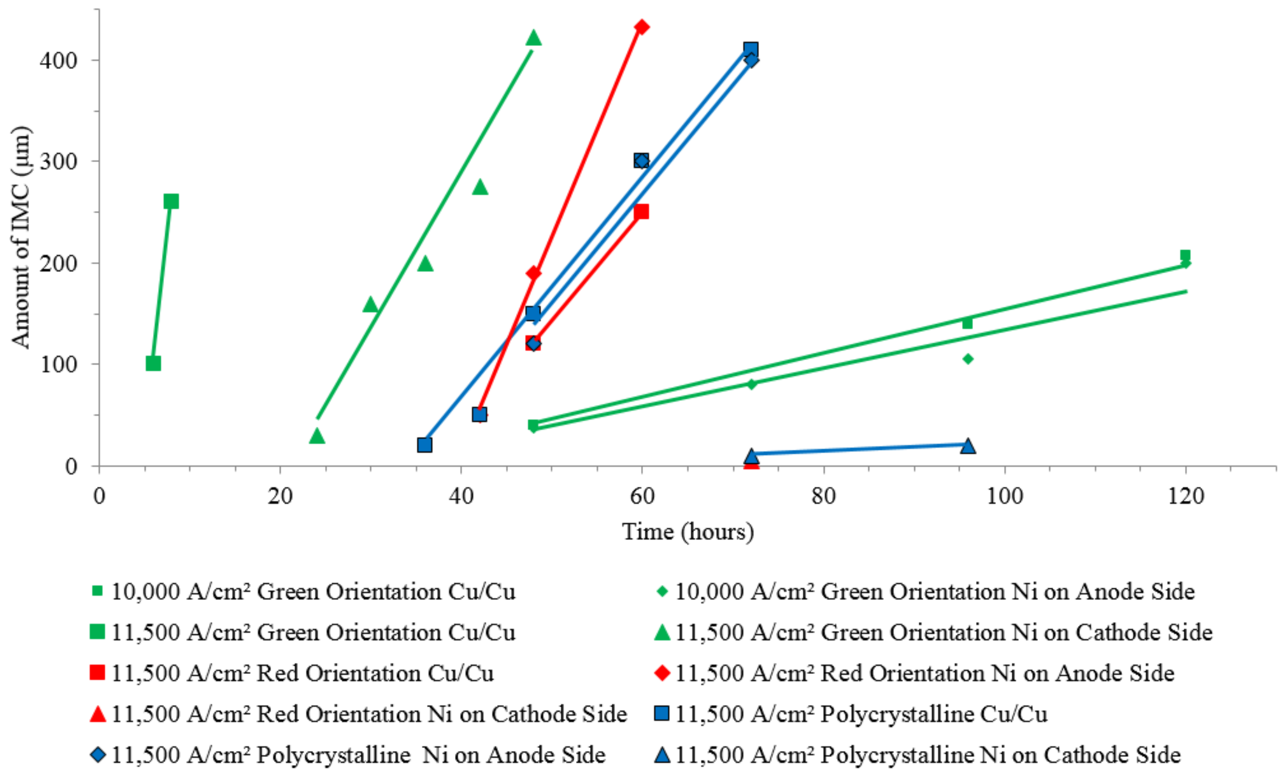

Figure 21: The measured thickness (x) of the Cu_6Sn_5 intermetallic layer plotted as a function of time for samples tested in prior works.

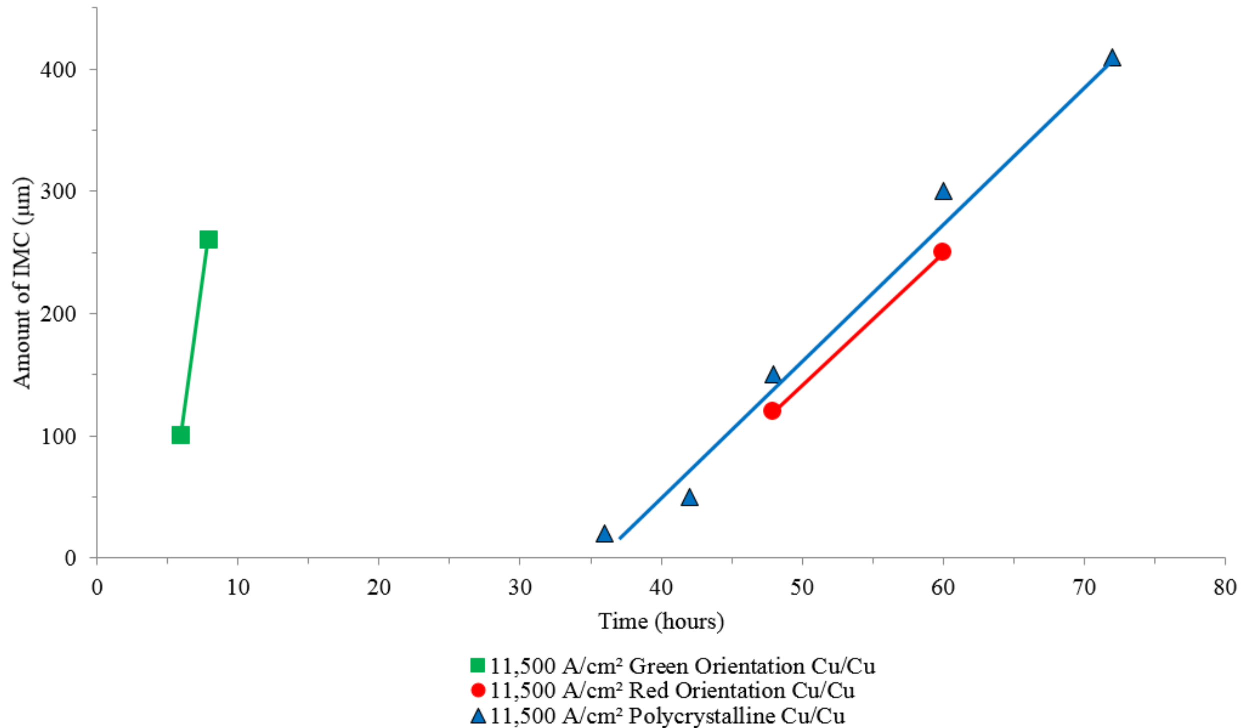

Figure 22: The measured thickness (x) of the Cu_6Sn_5 intermetallic layer plotted as a fuction of time for single crystalline and polycrystalline samples tested at 11,500A/cm2.

Single Crystalline Samples

The incubation period for "green" and "red" single crystalline oriented samples was observed and their timelines are shown in Figures 23 and 24, respectively. The figures show that IMC particles (Cu_3Sn and Cu_6Sn_5) nucleate and grow in the bulk of the joint, while a thin IMC layers exists on the anode and cathode side of the joint. Once the IMC layer on the cathode side of the joint breaks or dissolves, the IMC at the anode side of the joint begins to grow, and Cu_6Sn_5 particles in the bulk dissolve leaving small Cu_3Sn particles in the remaining solder joint.

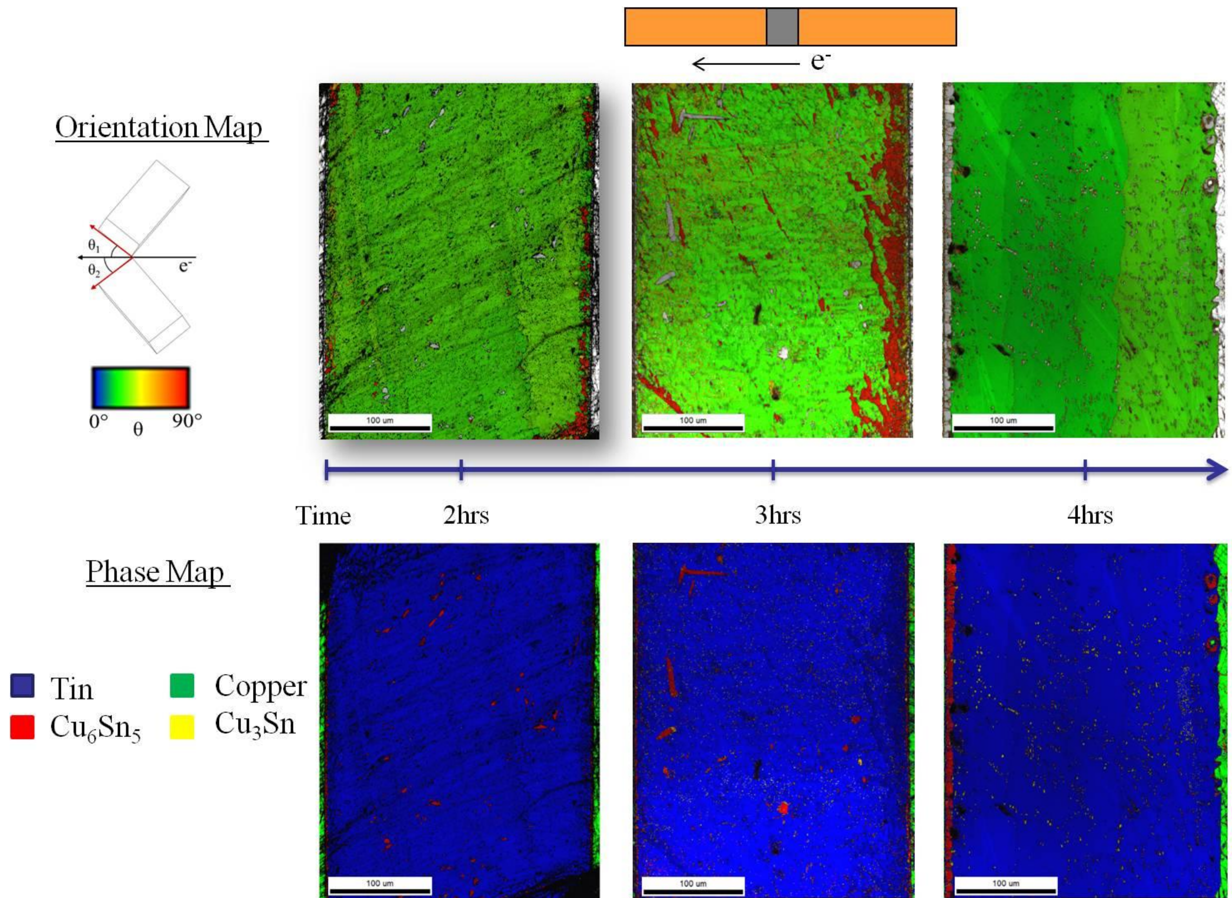

Figure 23: Green oriented single crystalline samples tested at 11,500A/cm2 for varying lengths of time.

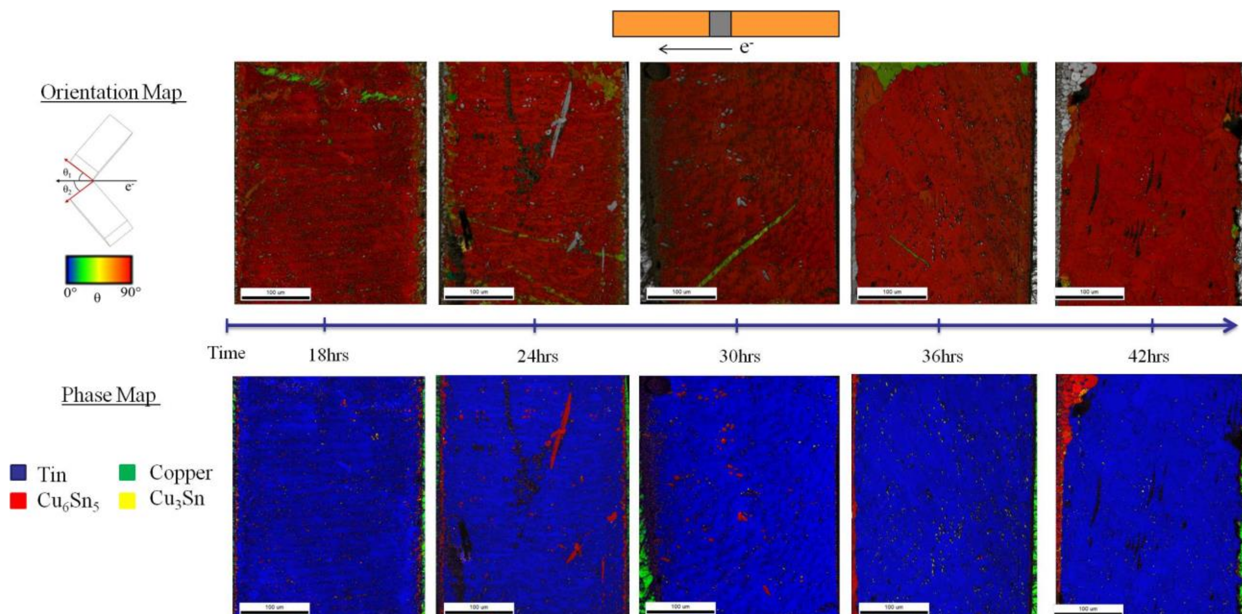

Figure 24: Red oriented single crystalline samples tested at 11,500A/cm2 for varying lengths of time.

Polycrystalline Samples

The incubation period for polycrystalline samples was also looked at and its timeline is shown in Figure 25. The Figure illustrate that before the intermetallic at the Cu/Sn interface starts growing, Cu_3Sn and Cu_6Sn_5 nucleate and grow in the bulk of the grains and in the grain boundaries. These IMC particles seem to nucleate in or between grains that precede lower diffusivity grains (i.e. if Cu is swept through a yellow oriented grain and a red grain is next, the IMC particles will nucleate in the yellow grain or between them). The intermetallic on the anode side of the interconnect then starts growing when the small intermetallic layer on the cathode side of the interconnect breaks or dissolves. Once the IMC at the anode interface of the joint begins to grow, Cu_6Sn_5 particles dissolve leaving small Cu_3Sn particles in the remaining solder joint.

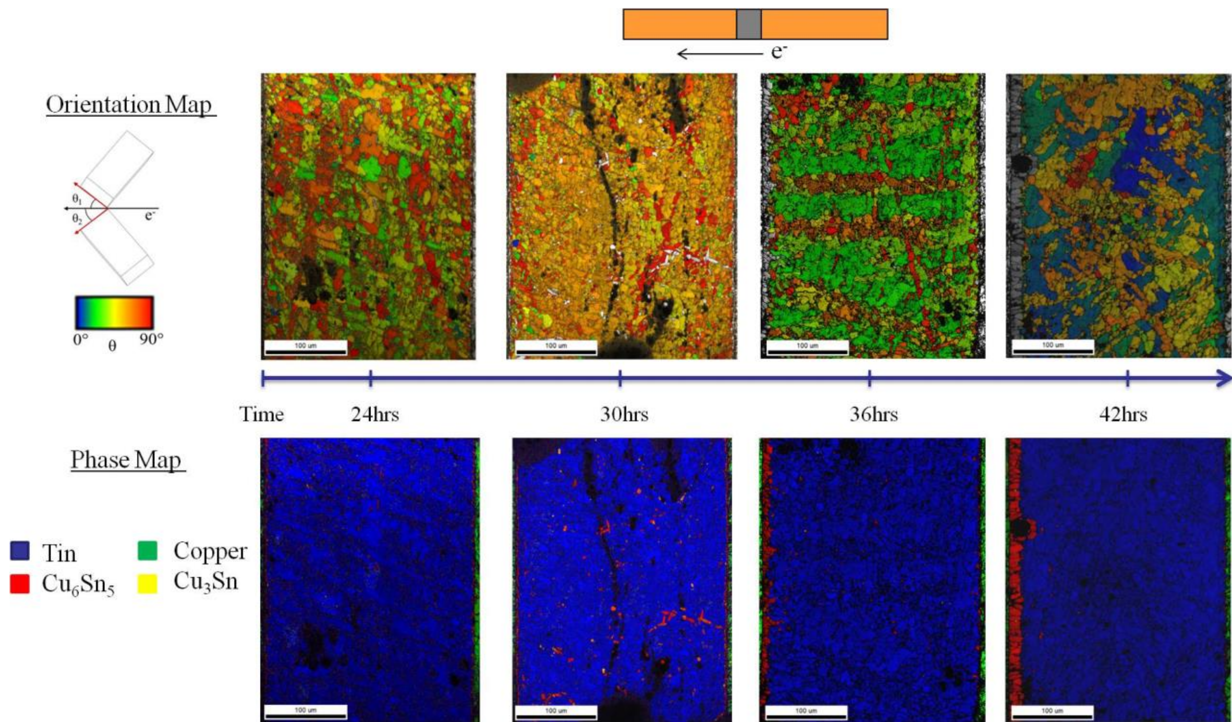

Figure 25: Polycrystalline samples tested at 11,500A/cm2 for varying lengths of time.

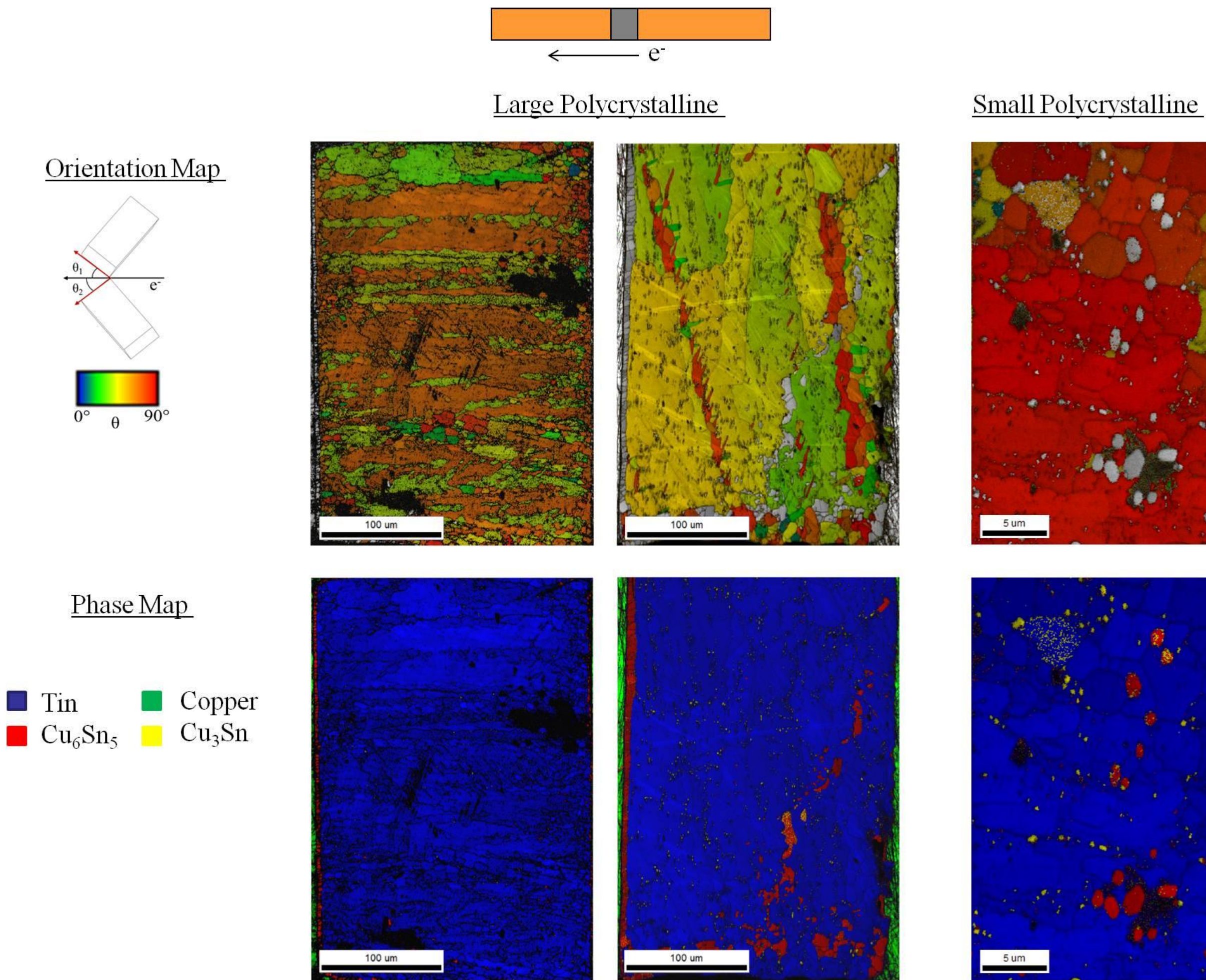

Figure 26: Polycrystalline (large and small) samples tested at 11,500A/cm2 for 36 hours.

Chapter 5: Discussion

Electromigration Equation

Growth Rate Evaluation

The growth rate of the IMC layer on the anode side of the joint interface should be determined by the rate of delivery of Cu through the solder to the growing interface. Cu diffuses by two parallel mechanisms: normal entropic diffusion down a concentration gradient (if one exists) and current-driven diffusion via electromigration. At sufficiently high current densities the electromigration should dominate, in which case there will be no significant concentration gradient through the body of the solder.

To test whether electromigration dominates in the test conditions used here, we used EDS analysis in a SEM and WDS analysis in an EPMA to profile the Cu concentration through the joint. The results document a nearly constant Cu concentration through the joints. However, an

exact value for the Cu concentration could not be measured due to the existence of micron sized IMC particles dispersed through the joints. The presence of the Cu_6Sn_5 precipitates suggests that the matrix concentration should be the concentration in equilibrium with the precipitate phase, and can, therefore, be inferred from the phase diagram. Consequently, we used the Cu solubility limit, confirmed by Moon, et al [31], for the Cu concentration values. Since the temperature is also constant through the joint, the growth rate is fully determined by the electromigration flux of Cu to the growing interface.

In the absence of a concentration gradient the electromigration flux of Cu atoms through bulk Sn is given by the following relation [7,8]:

$$J_{Cu} = c\left[\frac{D_{Cu}^{Sn}}{kT}\right]z^{*}e\rho j \qquad (9)$$

Where c is the concentration of Cu in Sn, D_{Cu}^{Sn} is the diffusivity of Cu in Sn, T is the temperature, z^* is the effective charge of Cu in Sn, e the electron charge, ρ the resistivity and j the current density. This can be re-written in the simpler form

$$J_{Cu} = cD_{Cu}^{*}j \qquad (10)$$

where the "effective diffusivity" for electromigration is

$$D_{Cu}^{*} = \left[\frac{D_{Cu}^{Sn}}{kT}\right]z^{*}e\rho \qquad (11)$$

Diffusivity Dependence on Orientation

The effective diffusivity, D^*, for Cu in Sn is a function of temperature and, in the case of single-crystal Sn, is also a function of the direction of the imposed current. In fact, D^* is a second-order tensor that has the tetragonal symmetry of the Sn crystal. When referred to the crystal axes of Sn it has two independent elements, D_c^*, which governs the flux along the c-axis, and D_a^*, which govern the (isotropic) flux in the perpendicular plane. Eq. (11) holds, with the appropriate value of D^*, which depends on the orientation between the electron flow and the c-axis.

To understand the effective diffusivity of the polycrystalline samples under current stress, recall that the Cu concentration in the joint is constant in both space and time. Since the concentration does not change with time we have, via Fick's Second Law, for a uniaxial flux

$$\frac{\partial c}{\partial t} = 0 = \frac{\partial}{\partial x}\left(J_{Cu}\right) \qquad (12)$$

from which it follows that $\boldsymbol{J_{Cu}}$ is constant. The flux is determined by Fick's First Law which, given the contribution of the electromigration flux, reads

$$J_{Cu} = -D\left(\frac{\partial c}{\partial x}\right) + c\left(\frac{D}{kT}\right) z^* eE \tag{13}$$

To achieve a spatially uniform concentration in a fine-grained polycrystal, the local average of the gradient must vanish. We have, hence,

$$\left\langle \frac{\partial c}{\partial x} \right\rangle = 0 = J_{Cu}\left\langle \frac{1}{D} \right\rangle - \frac{c}{kT} z^* eE \tag{14}$$

or

$$J_{Cu} = c\frac{D'}{kT} z^* eE = c\frac{D'}{kT} z^* e\rho j \tag{15}$$

where the polycrystal diffusivity, *D'*, is determined by the average value of 1/D:

$$\left(D'\right)^{-1} = \left\langle \frac{1}{D} \right\rangle = \frac{1}{D_c} + \frac{2}{D_a} \tag{16}$$

where D_c is the diffusivity along the c-axis and D_a is the diffusivity along the perpendicular axes. It should be obvious from equation (16) that the value of the polygranular is dominated by the value of D_a, which is both smaller than D_c and has twice the weight. It follows that $D' \sim D_a$, as is observed experimentally.

Calculation of the Effective Charge

To find the growth rate of IMC for a given value of the flux, we need to know the increase in the IMC layer thickness per Cu atom. Using the lattice structure of Cu_6Sn_5 [30,31], the intermetallic volume associated with a single Cu atom can be calculated, and it is δv = 3.24x10^{-29} m^3/cu atom. Accordingly, the growth rate is

$$\frac{dx}{dt} = J_{Cu}\delta v = (cD^*_{Cu} j)\delta v \tag{17}$$

If we use the anisotropic diffusivity measured by Dyson, et al [14] and the anisotropic resistivity [18] (ignoring the small change in resistivity with temperature), then Eqs. (11) and (17) become an equation for the only remaining unknown, the effective charge, z*. Our z* values for the various sample configurations are shown in Table 3, along with values for the effective diffusivity, D*, and Dz*.

Table 3: The calculated effective charge, z*, diffusivity of Cu in Sn times the effective charge, Dz*, and effective diffusivity, D*, for various sample conditions.

Specimen	Z*	DZ* (m^2/s)	D* (m^3/sA)
Green Orientation			
Cu/Cu, 10K A/cm², 150°C	0.11	$8.99x10^{-11}$	$3.21x10^{-16}$
Cu/Cu, 11.5K A/cm², 160°C	4.19	$4.00x10^{-9}$	$1.40x10^{-14}$
Ni on Anode, 10K A/cm², 150°C	0.1	$8.37x10^{-11}$	$2.99x10^{-16}$
Ni on Cathode, 11.5K A/cm², 160°C	0.55	$5.23x10^{-10}$	$1.82x10^{-15}$
Red Orientation			
Cu/Cu, 11.5K A/cm², 160°C	20.25	$4.98x10^{-10}$	$1.33x10^{-15}$
Ni on Anode, 11.5K A/cm², 160°C	22.11	$5.43x10^{-10}$	$1.46x10^{-15}$
Ni on Cathode, 11.5K A/cm², 160°C	0.24	$5.97x10^{-12}$	$1.60x10^{-17}$
Polycrystalline			
Cu/Cu, 11.5K A/cm², 160°C	12.92	$4.70x10^{-10}$	$1.39x10^{-15}$
Ni on Anode, 11.5K A/cm², 160°C	13.18	$4.80x10^{-10}$	$1.42x10^{-15}$
Ni on Cathode, 11.5K A/cm², 160°C	0.47	$1.72x10^{-11}$	$5.06x10^{-17}$

One interesting feature of the data shown in Tables 2 and 3 is the comparison between the values obtained for the polycrystalline and the “red” single crystal samples. As shown in Table 2, the growth rates for the “red” and polycrystalline samples are almost identical for both the Cu/Cu metallization and the Cu/Ni metallization (Ni on the anode side). The analysis leading to eq. (16) largely explains this phenomenon; the average diffusivity in the polycrystalline samples is close to that in the “red” samples. However, the growth rates in the two cases are even closer than the comparative diffusivities predict. It appears that the effective charge, z*, also varies slightly between the two specimen types, compensating for the small difference in diffusivity.

The comparative values shown in the tables for the "red" and polycrystalline samples with the Ni/Cu metallization (Ni on the cathode side) are not so close. However, as shown in Figure 20, the two growth rates in this case are very small, and were computed from only two data points, so the differences may not be meaningful.

These results suggest that polycrystalline interconnects may be as useful in slowing electromigration related damage and IMC growth as samples that have the c-axis orientated perpendicularly. Since presently there is no known way to control the single crystalline orientation of these samples on an industrial scale, the finding that polycrystalline samples behave like the 'desired' single crystalline orientation is significant. By using polycrystalline interconnects, the electromigration lifetime of interconnects could be prolonged; although future work is needed to explore this phenomenon further.

Furthermore, the apparently strong directional dependence of z^*, and D* as it depends on z*, is interesting. Since z^* reflects the response of the migrating atom to the electric current, it is not surprising that it should depend on direction. In one way, z* can be thought of as a measure of the force the electron wind exerts on the atoms to migrate them along the direction of the electron wind. Consequently, a higher z* for a perpendicular c axis / e- flow relationship means that the electron wind exerts relatively more force on the Cu atom to drive it along the direction of the electron wind, which is not necessarily unexpected given the lower diffusivity. That is to say that since a Cu atom has more difficulty jumping from site to site, the relative effect of the momentum transfer from the electron wind is greater, and therefore the value of z* is higher.

Given the small change in growth rate between samples with a Ni layer on the anode to those with no Ni layer, it is unsurprising that the z* values are quite similar. Samples with a Ni layer on the cathode had a very small z*, which can be explained by the strong dependence of z* on the growth rate of IMC. The Ni layer on the cathode greatly reduces the IMC growth rate, and in turn, gives us a much lower value of z*. Still, the magnitude of the difference may be surprising, and should be re-tested in further work. Even a small error in the values we have used for the anisotropic activation energy for diffusion (from Dyson, et al [14]) could produce a significant change in the anisotropy of z^*.

Incubation Period for Intermetallic Growth

When molten solder comes in contact with the Cu surface it is adhering to, thin layers of Cu_3Sn and Cu_6Sn_5 form in the interface (ie. Sn - Cu_6Sn_5 - Cu_3Sn - Cu). During electromigration, the electron wind pushes Cu ions from the Cu surface into the solder. However, before the Cu ions can enter the solder joint, they must pass through the Cu_3Sn and Cu_6Sn_5 IMC layers that exist at the cathode interface of the joint. The existence of an initial period of time where very little to no Cu seems to enter the joint suggests that these IMCs act as a barrier to Cu flow. This is consistent with literature because the diffusivity of Cu in Cu_3Sn and Cu_6Sn_5 is lower than that of Cu in Sn. Over time, these layers of IMC at the cathode side of the joint dissolve creating openings for Cu ions to enter the solder joint and begin growing the IMC layer on the anode side.

Chapter 6: Conclusion

In the work reported above we explored the influence of crystal orientation on the growth of the interfacial intermetallic layer during electromigration in Cu||Sn||Cu solder joints. The samples used were thin, planar Sn-Ag-Cu (SAC) solder layers between Cu pads subject to a uniaxial current at uniform temperature. EBSD was used to characterize the microstructure. The tested samples included single crystal joints with c-axis nearly parallel to the current ("green" samples) and with c-axis perpendicular to the current ("red" samples) and polycrystalline samples. All sample configurations were tested without a Ni layer, and with a Ni layer at either the anodic or cathodic side of the interface. A current density and temperature of $1.15x10^4$ A/cm^2 and 160ºC, respectively, led to measurable intermetallic growth in "green", "red", and polycrystalline samples. The growth fronts were nearly planar and the growth rates constant (after an initial incubation period); the growth rates in the "green" samples were about 10x those in the "red" samples, which had growth rates very close to the polycrystalline samples. The Cu concentrations were constant within the joints during the tests, showing that the intermetallic growth is dominated by the electromigration flux. The measured growth rates and literature values for the diffusion of Cu in Sn were used to extract values for the effective charge, z^*, that governs the electromigration of Cu. All samples with a Ni layer at the cathode, where IMC growth was significantly suppressed, had very similar, small z* values (all less than 1). For all other sample configurations, the calculated value of z^* is significantly larger for polycrystalline samples and samples with a current perpendicular to the c-axis than samples with a current parallel to the c-axis. Somewhat surprisingly, the polycrystalline samples had IMC growth rates and effective diffusivity values very close to single crystalline samples with the c-axis perpendicular to the current flow.

References:

[1] N. R. C. Committee on Manufacturing Trends in Printed Circuit Technology, Linkages: Manufacturing Trends in Electronics Interconnection Technology, The National Academies Press, 2005.

[2] X. Linares, C. Kinney, K.O. Lee, J.W. Morris, *JEM* 43, 43 (2014)

[3] C. Kinney, X. Linares, K.O. Lee, J.W. Morris, *JEM* 42, 607 (2013)

[4] C. Kinney, J.W. Morris, T.K. Lee, K.C. Liu, *JEM* 38, 2585 (2009)

[5] C. Kinney, J.W. Morris, T.K. Lee, K.C. Liu, D. Towne, *JEM* 38 221 (2009)

[6] K. Yamanaka, Y. Tsukada, and K. Suganuma, *Microelectron Reliab.* 47, 1280 (2007)

[7] B.K. Chao, X. Zhang, S.H. Chae, P.s. Ho, *Microelectron Reliab.* 49, 253 (2009)

[8] H.B. Huntington, A.R. Grone, *J. Phys. Chem. Solids* 20, 76 (1961)

[9] T. Laurila, J. Karppinen, V. Vuorinen, A. Paul, M. Paulasto-Krockel *JEM* 40, 1517 (2011)

[10] W. Peng, E. Monlevade, M. Marques, *Microelectron Reliab.* 47, 2161 (2007).

[11] J. Shi, H.B. Huntington, *J. Phys. Chem. Solids* 48, 696 (1987)

[12] B. Chao, S.H. Chae, X. Zhang, K.H. Lu, J. Im, P.S. Ho, *Acta Mat* 55, 2805 (2007)

[13] G.A. Sullivan, *Phys. Rev.* 154, 605 (1967)

[14] B.F. Dyson, T.R. Anthony, D. Turnbull, *J. Applied Physics* 38, 3408 (1967)

[15] D.C. Yeh, H.B. Huntington, *Phys Rev Lett*, 53, 1469 (1984)

[16] K.O. Lee, J.W. Morris, F. Hua, *Metallurgical and Materials Trans. A* 41A, 1805 (2010)

[17] T.K. Lee, B. Liu, B. Zhou, T. Bieler, K.C. Liu, *JEM* 40, 1895 (2011)

[18] T.H. Laby, G.W.C. Kaye, "Tables of Physical & Chemical Constants", 15th ed. (Longman, 1986), pp. 119

[19] M. Abtew, & G. Selvaduray, *Materials Science and Engineering: Reports* 27, 95-141 (2000)

[20] T.P. Vianco, Development of Alternatives to Lead-Bearing Solders, "Proceedings of the Technical Program on Surface Mount International", (San Jose, CA, 1993)

[21] R.E. Reed-Hill, "Physical Metallurgy Principles", PWS Publishing Company, (Massachusetts, 1994), pp. 306-307.

[22]E. Königsberger, Improvement of excess parameters from thermodynamic and phase diagram data by a sequential Bayes algorithm, CALPHAD: Comput. Coupling Phase Diagrams Thermochem., Vol. 15, 1991, p 69-78

[23] M. L. Liu, & A. M. Ahmad, Interfacial Reaction of Sn-Ag-Cu Lead-Free Solder Alloy on Cu: A Review. *Advances in Materials Science and Engineering* , 1-11 (2013)

[24] J. Wang, H.S. Liu, L.B. Liu, and Z.P. Jin, Thermodynamic description of the Sn-Ag-Au ternary system, CALPHAD: Comput. Coupling Phase Diagrams Thermochem., Vol. 31, 2007, p 545-552

[25] Grone AR. J Phys Chem Solids 1961;20:88.

[26] Sullivan GA. J Phys Chem Solids 1967;28:347.

[27] Grimme D. Atomic transport in solids and liquids. Tubingen: Verlag der Zeitschrift fur Naturforschung; 1971.

[28] Hsieh MY, Huntington HB. J Phys Chem Solids 1978;39:867.

[29] Chao BHL, Ho PS. 2007. Investigation of diffusion and electromigration parameters for Cu-Sn intermetallic compounds in Pb-free solders using simulated annealing. *Acta Mater. 55:2805–14*

[30] W.H. Wu, H.L. Chung, C.N. Chen, C.E. Ho, *JEM* 38 2563 (2009)

[31] K.W. Moon, W.J. Boettinger, U.R. Kattner, F.S. Biancaniello, C.A. Handwerker, *JEM* 29, 1122 (2000)

[32] A.K. Larsson, L. Stenberg, S. Lidin, *Acta Cryst.* B50, 636 (1994)